Combined open-loop and funnel control for underactuated multibody systems

Thomas Berger · Svenja Otto · Timo Reis · Robert Seifried

Abstract We consider tracking control for multibody systems which are modelled using generalized coordinates. Utilizing the two degree of freedom approach to controller design we combine a feedforward with a feedback controller. The feedforward control input is computed using the method of servo-constraints, which relies on an inverse model of the system. The feedback control input is generated by a dynamic output feedback which consists of the combination of a funnel controller with a funnel pre-compensator. This feedback controller is model-free and hence inherently robust. The control design is restricted to multibody systems with relative degree two or three which have input-to-state stable internal dynamics. In the main result we prove that the proposed controller is able to guarantee prescribed performance of the tracking error even in the presence of uncertainties and disturbances. We illustrate the application of the control design by a mass on car system (single-input, single-output) and a planar robotic manipulator (2-input, 2-output). In the case of relative degree two, these systems contain an unknown friction term.

Thomas Berger, Timo Reis
Department of Mathematics, Universität Hamburg, Bundesstraße 55, 20146 Hamburg, Germany
E-mail: {thomas.berger, timo.reis}@uni-hamburg.de

Svenja Otto, Robert Seifried
Institute of Mechanics and Ocean Engineering, Hamburg University of Technology, Eißendorfer Straße 42, 21073 Hamburg, Germany
E-mail: {svenja.otto, robert.seifried}@tuhh.de

1 Introduction

In the present paper we study the two degree of freedom approach to controller design, see e.g. [42]. In this approach, an open-loop (feedforward) controller and a feedback controller are independently designed to achieve a certain control task, such as tracking of a reference signal. The feedforward control input is designed such that exact tracking for a reference model of the system is achieved. For the computation of the feedforward control input we will use the servo-constraints approach, which is based on an inverse model of the system.

Since modelling errors, uncertainties, noise and disturbances which influence the system are expected, a feedback control loop is incorporated on top of the feedforward control part. The feedback loop is essentially used to stabilize the system around the prescribed reference trajectory. A favorable choice seems to be a model-free feedback control design, since such a controller is inherently robust. Additionally, from a practical point of view it is often desirable that the tracking error stays within a prescribed range of tolerance. To achieve this, even in the presence of uncertainties and disturbances, we will use a funnel controller. Since a standard funnel controller requires the availability of the derivatives of the outputs, we utilize a recently developed combination of a funnel controller with a funnel pre-compensator.

Details of the considered system class and the proposed control methodology are given in the following.

1.1 Nomenclature

$\mathbb{R}_{\geq 0}$	$= [0, \infty)$
$\mathbf{Gl}_n(\mathbb{R})$	the group of invertible matrices in $\mathbb{R}^{n \times n}$
$\mathscr{L}^\infty_{\mathrm{loc}}(I \to \mathbb{R}^n)$	the set of locally essentially bounded functions $f : I \to \mathbb{R}^n$, $I \subseteq \mathbb{R}$ an interval
$\mathscr{L}^\infty(I \to \mathbb{R}^n)$	the set of essentially bounded functions $f : I \to \mathbb{R}^n$
$\|f\|_\infty$	$= \mathrm{ess} \sup_{t \in I} \|f(t)\|$
$\mathscr{W}^{k,\infty}(I \to \mathbb{R}^n)$	the set of k-times weakly differentiable functions $f : I \to \mathbb{R}^n$ such that $f, \dots, f^{(k)} \in \mathscr{L}^\infty(I \to \mathbb{R}^n)$
$\mathscr{C}^k(V \to \mathbb{R}^n)$	the set of k-times continuously differentiable functions $f : V \to \mathbb{R}^n$, $V \subseteq \mathbb{R}^m$
$\mathscr{C}(V \to \mathbb{R}^n)$	$= \mathscr{C}^0(V \to \mathbb{R}^n)$
$f\|_W$	restriction of the function $f : V \to \mathbb{R}^n$ to $W \subseteq V$

1.2 System class

We consider multibody systems which are modelled using generalized coordinates. If no kinematic loops are present in the system, it is always possible to select such a set of generalized coordinates q and generalized velocities v to describe the kinematics. Thus, the Newton and Euler equations of each body are projected onto the direction of free motion by d'Alemberts principle. This eliminates the reaction forces and yields the equations of motion in minimal coordinates

$$
\begin{aligned}
\dot{q}(t) &= v(t), \\
M(q(t)) \dot{v}(t) &= g(t, q(t), v(t)) + B(q(t)) u(t), \\
q(0) &= q^0 \in \mathbb{R}^n, \quad v(0) = v^0 \in \mathbb{R}^n,
\end{aligned} \tag{1}
$$

with

 – the generalized mass matrix $M \in \mathscr{C}^1(\mathbb{R}^n \to \mathbf{Gl}_n(\mathbb{R}))$,
 – the generalized forces $g \in \mathscr{C}^1(\mathbb{R} \times \mathbb{R}^n \times \mathbb{R}^n \to \mathbb{R}^n)$,
 – the input distribution matrix $B \in \mathscr{C}(\mathbb{R}^n \to \mathbb{R}^{n \times m})$.

The functions $u : \mathbb{R} \to \mathbb{R}^m$ are the inputs that influence the multibody system (1) in the affine form $B(q(t)) u(t)$, which has the interpretation of a force or torque whose intensity is given by $u(t)$ and the direction is given by $B(q(t))$. However, in practical applications forces and torques are hard to actuate, hence secondary velocity and position control loops are usually used. In particular, standard industrial actuators are typically velocity controlled and not force controlled. The secondary control loops of the actuator dynamics may lead to different system properties, such as a higher relative degree, cf. [34, Sec. 4.4]. In the present paper, for the sake of simplicity, we assume that the actuators are force/torque controlled and that the multibody system is given in the form (1).

The system output corresponding to (1) is usually defined in terms of the generalized coordinates, i.e.,

$$
y(t) = h(q(t)), \tag{2}
$$

where $h \in \mathscr{C}^3(\mathbb{R}^n \to \mathbb{R}^m)$. If it is possible to efficiently measure velocities, then output structures of the form $y(t) = h(q(t), v(t))$ are feasible. However, we restrict ourselves to an output of the form (2) in the present paper.

The generalized forces g usually encompass several terms, including applied forces, Coriolis, centrifugal and gyroscopic forces. Here, we put special emphasis on friction. Friction is a tangential force between two surfaces which can move relative to each other with relative velocity v_{rel}. Two friction regimes are distinguished, see [21, Chap. 9]. In case of no relative motion $v_{rel} = 0\,\mathrm{m/s}$, static friction occurs. In that case, the friction force F_R is a reaction force, which has to be computed. The system is in the static friction regime if the friction force F_R satisfies

$$
|F_R| < F_0 = \mu_0 N, \tag{3}
$$

where N denotes the normal force between the two surfaces and μ_0 describes the static friction coefficient. The friction coefficient depends on many parameters such as surface material, lubrication, temperature and others. If (3) does not hold, then the maximum static friction force cannot withstand the other applied forces and relative motion occurs. Then, the system is in the sliding friction regime with $v_{rel} > 0\,\mathrm{m/s}$. Then, the friction force F_R is an applied force acting in opposite direction of v_{rel}. There are many different friction models applicable for different simulation goals, see e.g. [3]. Here, we choose a simple friction model in order to show the feedback controller performance in the presence of friction. For the case $v_{rel} > 0\,\mathrm{m/s}$, friction is an applied force and is here calculated with

$$
F_R(v_{rel}) = \left(F_C + (F_0 - F_C) e^{-c_v |v_{rel}|} \right) \mathrm{sgn}(v_{rel}) + c_T v_{rel}, \tag{4}
$$

where F_C denotes the Coulomb friction $F_C = \mu N$ with the sliding friction coefficient μ. This models the Stribeck curve, see e.g. [3,32]. The transition from the maximum static friction F_0 to Coulomb friction F_C is defined by the coefficient c_v. For larger relative velocities, there is a linear relationship between relative velocity and friction force, modelled by the coefficient c_T. A qualitative example with $F_0 = 10\,\mathrm{N}$, $F_C = 8\,\mathrm{N}$, $c_v = 0.5$ and $c_T = 0.05\,\mathrm{kg/s}$ is shown in Figure 1.

The transition from static to sliding friction needs special attention for numerical implementation, see e.g. [32]. Additional to solving the equivalent static or dynamic equations in the respective regimes and checking (3) in the static regime, here the static regime around a small zone $|v_{rel}| <$
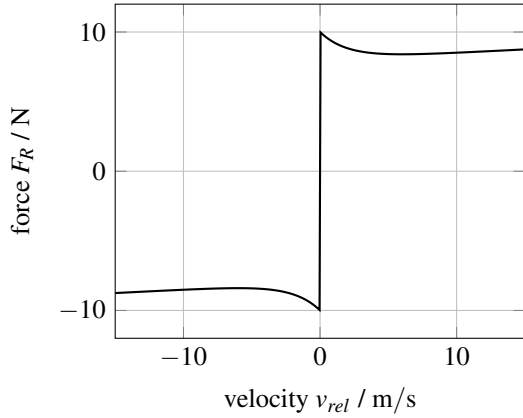
Fig. 1: Qualitative graph of sliding friction.

v_{th} is approximated by a steep line, such that

$$F_R(v_{rel}) =$$
$$\begin{cases} \left(F_C + (F_0 - F_C)\,e^{-c_v|v_{rel}|}\right)\operatorname{sgn}(v_{rel}) + c_T v_{rel}, & |v_{rel}| \geq v_{th} \\ \dfrac{v_{rel}}{v_{th}}\left(F_C + (F_0 - F_C)\,e^{-c_v v_{th}} + c_T v_{th}\right), & |v_{rel}| < v_{th}. \end{cases}$$
$$(5)$$

This contributes a stiff part to the dynamic equations (1).

1.3 Relative degree

An important property of the system (1), (2) is its relative degree, which, roughly speaking, is the number of derivatives of the output needed so that the input appears explicitly. For the output y as in (2) we obtain

$$\dot{y}(t) = h'\big(q(t)\big)\,\dot{q}(t) = \underbrace{h'\big(q(t)\big)}_{=:H(q(t))} v(t),$$

$$\ddot{y}(t) = H\big(q(t)\big)\dot{v}(t) + \bar{h}\big(q(t),v(t)\big)$$
$$= H\big(q(t)\big)M\big(q(t)\big)^{-1}\big[g\big(t,q(t),v(t)\big) + B\big(q(t)\big)u(t)\big]$$
$$\quad + \bar{h}\big(q(t),v(t)\big)$$

for $H \in \mathscr{C}^2(\mathbb{R}^n \to \mathbb{R}^{m \times n})$ and $\bar{h} \in \mathscr{C}^1(\mathbb{R}^{2n} \to \mathbb{R}^m)$ given by

$$\bar{h}(q,v) = \big(H'(q)v\big)v, \quad q,v \in \mathbb{R}^n.$$

We stress that $H'(q)$ is a tensor of third order for every $q \in \mathbb{R}^n$ and, correspondingly, $H'(q)v \in \mathbb{R}^{m \times n}$ for all $v \in \mathbb{R}^n$. Obviously the input u appears in the equation for $\ddot{y}$ provided that $H\big(q(t)\big)M\big(q(t)\big)^{-1}B\big(q(t)\big) \neq 0$. We stress that the rank of the matrix $H(q)M(q)^{-1}B(q)$ is also used as a measure for the system configuration, see [12,40]. If

$H\big(q(t)\big)M\big(q(t)\big)^{-1}B\big(q(t)\big) = 0$ we may compute

$$y^{(3)}(t) = \Big[H\big(q(t)\big)M\big(q(t)\big)^{-1}\frac{\partial g}{\partial v}\big(t,q(t),v(t)\big)$$
$$\quad + \frac{\partial \bar{h}}{\partial v}\big(q(t),v(t)\big)\Big]M\big(q(t)\big)^{-1}B\big(q(t)\big)u(t) + G\big(t,q(t),v(t)\big)$$

for some $G \in \mathscr{C}(\mathbb{R} \times \mathbb{R}^n \times \mathbb{R}^n \to \mathbb{R}^m)$. Higher relative degrees are possible, but we restrict ourselves to the following two cases here: The multibody system (1) with output (2) is said to have *relative degree*

(i) $r = 2$, if $H(q)M(q)^{-1}B(q) \in \mathbf{Gl}_m(\mathbb{R})$ for all $q \in \mathbb{R}^n$;
(ii) $r = 3$, if $H(q)M(q)^{-1}B(q) = 0$ and

$$\Big[H(q)M(q)^{-1}\frac{\partial g}{\partial v}(t,q,v) + \frac{\partial \bar{h}}{\partial v}(q,v)\Big]M(q)^{-1}B(q) \in \mathbf{Gl}_m(\mathbb{R})$$

for all $(t,q,v) \in \mathbb{R} \times \mathbb{R}^n \times \mathbb{R}^n$.

The above definition coincides with the concept of a *strict and uniform relative degree* for time-varying nonlinear systems introduced in [25]. Of course it is possible that, for instance, $H(q)M(q)^{-1}B(q)$ is neither invertible (everywhere or at some points) nor zero, but has constant rank. Then it is possible to extend the concept of relative degree to that of a (local) *vector relative degree*, see [29]; note that a strict relative degree r implies that the vector relative degree is $(r,\dots,r)$. For systems of differential-algebraic equations (DAEs) even a negative relative degree is possible, cf. [4].

Note that, if the output is simply a linear combination of the generalized coordinates, i.e., $h(q) = Cq$ for some $C \in \mathbb{R}^{m \times n}$, then $H(q) = C$ and $\bar{h}(q,v) = 0$. In this case, system (1), (2) has relative degree

– $r = 2$, if $CM(q)^{-1}B(q) \in \mathbf{Gl}_m(\mathbb{R})$ for all $q \in \mathbb{R}^n$, and
– $r = 3$, if $CM(q)^{-1}B(q) = 0$ and

$$CM(q)^{-1}\frac{\partial g}{\partial v}(t,q,v)M(q)^{-1}B(q) \in \mathbf{Gl}_m(\mathbb{R})$$

for all $(t,q,v) \in \mathbb{R} \times \mathbb{R}^n \times \mathbb{R}^n$.

1.4 Control methodology

We follow a popular controller design for mechanical systems by combining a feedforward controller with a feedback controller (cf. e.g. [42]), which are both designed independently for tracking of a reference trajectory $y_{\mathrm{ref}} \in \mathscr{W}^{r,\infty}(\mathbb{R}_{\geq 0} \to \mathbb{R}^m)$, where r is the relative degree of the multibody system (1), (2). The feedforward control input u_{ff} is designed using a reference (inverse) model of the system. The feedback control is applied to the actual system, which may deviate from the reference model, and provides the feedback control input u_{fb}. The situation is depicted in Figure 2.
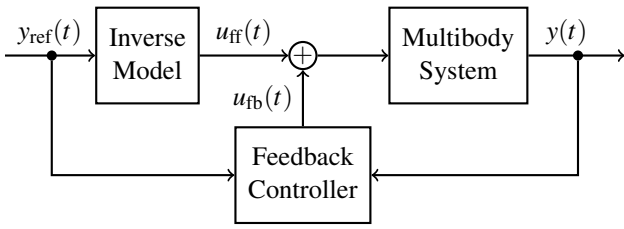
Fig. 2: Two degree of freedom control approach for multi-body systems.

In the present paper, the feedforward control input u_{ff} is computed using the method of servo-constraints which was introduced in [11], see also the extensions in [12,13]. In this framework the equations of motion of the multibody system (1) are extended by constraints enforcing the system output (2) to stay on the reference trajectory y_{ref}. Due to these constraints, the resulting system is a set of DAEs which is solved numerically for the inverse system. As a part of this numerical solution the feedforward control input u_{ff} is obtained. The details of the method are presented in Section 3.

Some typical examples of systems controlled by servo-constraints are rotary cranes [10], overhead gantry cranes [12,35] and (infinitely long) mass-spring chains [2, 19]. As shown in [16], adding servo-constraints to the system may result in DAEs with a higher differentiation index; see [14,20] and also [30] for a definition of the latter. This causes difficulties in the numerical solution and hence index reduction methods (cf. [23]) are frequently used. Essentially two different approaches are common: index reduction by projection onto the constrained and unconstrained directions as proposed in [12] and index reduction by minimal extension as proposed in [1,9].

The feedback control input u_{fb} is generated by a feedback loop using a dynamic output feedback of the form

$$\dot{z}(t) = F\big(t, z(t), y(t), y_{\text{ref}}(t), \ldots, y_{\text{ref}}^{(r-1)}(t)\big),$$
$$u_{\text{fb}}(t) = G\big(t, z(t), y(t), y_{\text{ref}}(t), \ldots, y_{\text{ref}}^{(r-1)}(t)\big), \quad (6)$$

for some $r > 0$. This feedback should be model-free in its design. Additionally, our aim is that in the closed-loop system, independent of the uncertainties and disturbances, the tracking error $e(t) = y(t) - y_{\text{ref}}(t)$ evolves within a prescribed performance funnel

$$\mathscr{F}_{\varphi} := \{ (t, e) \in \mathbb{R}_{\geq 0} \times \mathbb{R}^m \mid \varphi(t)\|L_o e\| < 1 \}, \quad (7)$$

which is determined by a matrix $L_o \in \mathbf{Gl}_m(\mathbb{R})$ and a function φ belonging to

$$\Phi_r := \left\{ \varphi \in \mathscr{C}^r(\mathbb{R}_{\geq 0} \to \mathbb{R}) \left| \begin{array}{l} \varphi, \dot{\varphi}, \ldots, \varphi^{(r)} \text{ are bounded,} \\ \varphi(\tau) > 0 \text{ for all } \tau > 0, \\ \text{and } \liminf_{\tau \to \infty} \varphi(\tau) > 0 \end{array} \right. \right\}. \quad (8)$$

Furthermore, all involved signals should remain bounded.

The funnel boundary is given by the reciprocal of φ, see Figure 3. The case $\varphi(0) = 0$ is explicitly allowed, meaning that no restriction is put on the initial value since $(0, e(0)) \in \mathscr{F}_{\varphi}$; the funnel boundary $1/\varphi$ has a pole at $t = 0$ in this case.
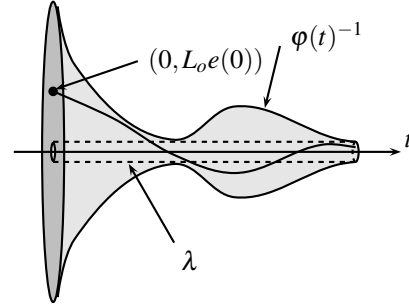

Fig. 3: Error evolution in a funnel $\mathscr{F}_{\varphi}$ with boundary $\varphi(t)^{-1}$.

An important property is that each performance funnel $\mathscr{F}_{\varphi}$ is bounded away from zero since boundedness of φ gives existence of $\lambda > 0$ such that $1/\varphi(t) \geq \lambda$ for all $t > 0$. We stress that the funnel boundary is not necessarily monotonically decreasing, which can be advantageous in some applications. Widening the funnel over some later time interval might be beneficial, e.g., when periodic disturbances are present or the reference signal varies strongly. For typical choices of funnel boundaries see e.g. [24, Sec. 3.2].

The reason to use the matrix L_o in (7) is to guarantee that $L_o e$ is physically "dimensionless". This is of particular interest whenever the to-be controlled system has multiple outputs with different physical dimensions. Then the multiplication with the matrix L_o ensures that no variables of different physical dimension are added while forming the norm $\|L_o e\|$. In the case where the physical dimensions of all outputs coincide, a typical choice for L_o is a scalar multiple of the identity matrix. A further discussion of this matrix can be found in Section 4.

The detailed design of a feedback controller of the form (6) which yields the feedback control input u_{fb} is presented in Section 4 using the combination of a recently developed funnel controller [5] with a funnel precompensator [8]. The funnel controller was originally developed in [27], see also the survey [26] and the references therein. It is an adaptive controller of high-gain type and has been successfully applied e.g. in temperature control of chemical reactor models [28], control of industrial servo-systems [22], DC-link power flow control [41], voltage and current control of electrical circuits [6], and control of peak inspiratory pressure [36].

1.5 Organization of the present paper

In Section 2 we introduce and investigate the concept of internal dynamics. For the multibody system (1), (2) we present a systematic approach to derive a coordinate transformation which leads to an inverse model where the internal dynamics are decoupled. As a crucial assumption on the internal dynamics we recall the concept of input-to-state stability. Exploiting the inverse model, the method of servo-constraints is presented in Section 3 which enables us to numerically obtain the feedforward control input u_{ff} which achieves exact tracking of the reference signal y_{ref} for the reference model without uncertainties and disturbances. If the latter are present, an additional feedback control loop which generates u_{fb} is necessary. As a feedback controller we use the combination of a funnel controller with a funnel pre-compensator that is presented in Section 4. We prove its feasibility and discuss the choice of design parameters. The application of the combination of feedforward control u_{ff} and feedback control u_{fb} is illustrated for some typical examples in Section 5.

2 Internal dynamics

In this section we investigate an important property of the multibody system (1), (2), that is its internal dynamics. Roughly speaking, the internal dynamics denote those dynamics of the system which are not observable from the output. Together with the zero dynamics, i.e., those dynamics which remain in the system when $y(t) = 0$, this concept goes back to Byrnes and Isidori [15], see also [29]. We aim to derive a nonlinear coordinate transformation of (1), (2) such that in the new system the internal dynamics are decoupled. We present a systematic approach to derive this transformation for the case of relative degree $r = 2$; in the case $r = 3$ the situation is more involved. Because of the decoupling, the transformed system also serves as basis for an *inverse model*, i.e., given a desired output $y_{\mathrm{ref}}(t)$ the corresponding input $u_{\mathrm{ff}}(t)$ (necessary to generate y_{ref}) can be computed.

An important property is the input-to-state stability of the internal dynamics, which was introduced by Sontag [43, 44] for nonlinear systems

$$\dot{x}(t) = f\big(x(t), u(t)\big), \quad x(0) = x^0 \in \mathbb{R}^n, \tag{9}$$

where $f \in \mathscr{C}(\mathbb{R}^n \times \mathbb{R}^m \to \mathbb{R}^n)$ is locally Lipschitz continuous in x. Denote with $x(\cdot; x^0, u) : [0, \omega) \to \mathbb{R}^n$ the unique maximal solution of (9) (cf. e.g. [45, § 10, Thm. VI]) for some $u \in \mathscr{L}^\infty_{\mathrm{loc}}(\mathbb{R}_{\geq 0} \to \mathbb{R}^m)$. We call (9) *complete*, if $\omega = \infty$ for all $x^0 \in \mathbb{R}^n$ and all $u \in \mathscr{L}^\infty_{\mathrm{loc}}(\mathbb{R}_{\geq 0} \to \mathbb{R}^m)$. Recall the fol-

lowing classes of functions:

$$\mathscr{K} := \{\alpha \in \mathscr{C}(\mathbb{R}_{\geq 0} \to \mathbb{R}_{\geq 0}) \,|\, \alpha(0) = 0,\ \alpha \text{ str. increasing}\},$$

$$\mathscr{K}_\infty := \{\alpha \in \mathscr{K} \mid \alpha \text{ unbounded}\},$$

$$\mathscr{K}\mathscr{L} := \left\{ \beta \in \mathscr{C}(\mathbb{R}^2_{\geq 0} \to \mathbb{R}_{\geq 0}) \,\left|\, \begin{array}{l} \beta(\cdot, s) \in \mathscr{K} \text{ for all } s \geq 0, \\ \lim_{s \to \infty} \beta(t, s) = 0 \text{ for all } t \geq 0 \end{array} \right. \right\}.$$

Definition 21 *The system* (9) *is called* input-to-state stable, *if there exist* $\beta \in \mathscr{K}\mathscr{L}$ *and* $\gamma \in \mathscr{K}_\infty$ *such that for all bounded* $u \in \mathscr{C}(\mathbb{R}_{\geq 0} \to \mathbb{R}^m)$ *and all* $x^0 \in \mathbb{R}^n$ *the solution* $x(\cdot; x^0, u) : [0, \omega) \to \mathbb{R}^n$ *of* (9) *satisfies that*

$$\forall t \in [0, \omega) : \ \|x(t)\| \leq \max\{\beta(\|x^0\|, t), \gamma(\|u\|_\infty)\}.$$

Note that in the above definition it is not explicitly required that $\omega = \infty$, however this is a direct consequence of input-to-state stability. If we would have $\omega < \infty$, then by input-to-state stability the set $\overline{\{(t, x(t)) \mid t \in [0, \omega)\}}$ would be a compact subset of $\mathbb{R} \times \mathbb{R}^n$, which is a contradiction. We stress that this does not imply that (9) is complete, since input-to-state stability considers only *bounded* inputs u, while completeness requires a global solution for every input.

In the next step we derive the internal dynamics of (1), (2) under the assumption of relative degree $r = 2$ or $r = 3$.

Case $r = 2$: Define the matrices

$$\mathscr{B}(q) := \begin{bmatrix} 0 & M(q)^{-1}B(q) \\ M(q)^{-1}B(q) & 0 \end{bmatrix} \in \mathbb{R}^{2n \times 2m},$$

$$\mathscr{C}(q, v) := \begin{bmatrix} h'(q) & 0 \\ H'(q)v & H(q) \end{bmatrix} \in \mathbb{R}^{2m \times 2n},$$

for $q, v \in \mathbb{R}^n$. Let $\Gamma(q) := H(q)M(q)^{-1}B(q) \in \mathbf{Gl}_m(\mathbb{R})$, then

$$\mathscr{C}(q, v)\mathscr{B}(q) = \begin{bmatrix} 0 & \Gamma(q) \\ \Gamma(q) & * \end{bmatrix}$$

is invertible for all $q, v \in \mathbb{R}^n$, hence

$$\forall q, v \in \mathbb{R} : \ \mathrm{rk}\,\mathscr{C}(q, v) = 2m.$$

Therefore, there exists $V : \mathbb{R}^{2n} \to \mathbb{R}^{2n \times (2n - 2m)}$ such that $\mathrm{im}\,V(q, v) = \ker \mathscr{C}(q, v)$ for all $q, v \in \mathbb{R}^n$. We assume that V is continuous and define

$$W(q, v) = V(q, v)^\dagger \left(I_{2n - 2m} - \mathscr{B}(q)\big(\mathscr{C}(q, v)\mathscr{B}(q)\big)^{-1}\mathscr{C}(q, v) \right),$$

which is continuous as well; note that $A^\dagger$ denotes the Moore-Penrose pseudoinverse of A. For later use we record that

$$\forall q, v \in \mathbb{R}^n : \ W(q, v)\mathscr{B}(q, v) = 0,\ W(q, v)V(q, v) = I_{2n - 2m}. \tag{10}$$

Denote the columns of $W(q,v)$ by $w_i(q,v)$ for $i = 1,\ldots,2n$ and assume that, for any closed path $\gamma \in \mathscr{C}([a,b] \to \mathbb{R}^{2n})$ the path integral satisfies

$$\int_a^b w_i\big(\gamma(t)\big)\|\dot{\gamma}(t)\|\,\mathrm{d}t = 0,$$

i.e., the vector field w_i is conservative. By the gradient theorem, there exists a scalar field $\Phi_i \in \mathscr{C}^1(\mathbb{R}^{2n} \to \mathbb{R})$ such that $\Phi_i'(q,v) = w_i(q,v)$. With $\Phi = (\Phi_1,\ldots,\Phi_{2n})^\top$ we obtain that the Jacobian of Φ equals W, i.e.,

$$\forall q,v \in \mathbb{R}^n: \ \Phi'(q,v) = W(q,v).$$

Now define $\psi \in \mathscr{C}^1(\mathbb{R}^{2n} \to \mathbb{R}^{2n})$ by

$$\psi(q,v) = \begin{pmatrix} h(q) \\ H(q)v \\ \Phi(q,v) \end{pmatrix}, \quad q,v \in \mathbb{R}^n. \tag{11}$$

Observe that the Jacobian is given by

$$\psi'(q,v) = \begin{bmatrix} \mathscr{C}(q,v) \\ W(q,v) \end{bmatrix}$$

and is invertible everywhere since

$$\begin{bmatrix} \mathscr{C}(q,v) \\ W(q,v) \end{bmatrix} \left[\mathscr{B}(q)\big(\mathscr{C}(q,v)\mathscr{B}(q)\big)^{-1}, V(q,v) \right] \overset{(10)}{=} \begin{bmatrix} I_{2m} & 0 \\ 0 & I_{2n-2m} \end{bmatrix}.$$

Therefore, ψ is a diffeomorphism and we may use it as a state space transformation of (1), (2) to new coordinates

$$\psi\big(q(t),v(t)\big) = \begin{pmatrix} y(t) \\ \dot{y}(t) \\ \Phi\big(q(t),v(t)\big) =: \eta(t) \end{pmatrix},$$

which gives

$$\begin{pmatrix} \dot{y}(t) \\ \ddot{y}(t) \\ \dot{\eta}(t) \end{pmatrix} = \begin{pmatrix} \dot{y}(t) \\ H\big(q(t)\big)M\big(q(t)\big)^{-1}g\big(t,q(t),v(t)\big)+\bar{h}\big(q(t),v(t)\big) \\ W\big(q(t),v(t)\big)\begin{pmatrix} v(t) \\ M\big(q(t)\big)^{-1}g\big(t,q(t),v(t)\big) \end{pmatrix} \end{pmatrix}$$

$$+ \begin{bmatrix} 0 \\ \Gamma\big(q(t)\big) \\ W\big(q(t),v(t)\big)\begin{bmatrix} 0 \\ M\big(q(t)\big)^{-1}B\big(q(t)\big) \end{bmatrix} \end{bmatrix} u(t). \tag{12}$$

Since

$$W(q,v)\begin{bmatrix} 0 \\ M(q)^{-1}B(q) \end{bmatrix} = W(q,v)\mathscr{B}(q)\begin{bmatrix} I_m \\ 0 \end{bmatrix} \overset{(10)}{=} 0,$$

it follows that (12) is equivalent to

$$\ddot{y}(t) = f_1\big(t,y(t),\dot{y}(t),\eta(t)\big) + \bar{\Gamma}\big(y(t),\dot{y}(t),\eta(t)\big)u(t), \\ \dot{\eta}(t) = f_2\big(t,y(t),\dot{y}(t),\eta(t)\big) \tag{13}$$

for some $f_1 \in \mathscr{C}(\mathbb{R} \times \mathbb{R}^{2n} \to \mathbb{R}^m)$, $f_2 \in \mathscr{C}(\mathbb{R} \times \mathbb{R}^{2n} \to \mathbb{R}^{2n-2m})$ and

$$\bar{\Gamma}(y_0,y_1,\eta) := \Gamma\big([I_n,0]\psi^{-1}(y_0,y_1,\eta)\big).$$

The second equation in (13) is called the *internal dynamics* of (1), (2), where η is the "state" and $(y,\dot{y})$ is the "input" of the internal dynamics. For the structural investigation of the internal dynamics, it turns out that f_2 should be bounded in t and that bounded parts of f_2 should be treated like additional inputs. With respect to all resulting inputs we may assume input-to-state stability.

Assumption 22 *We assume that the diffeomorphism $\psi \in \mathscr{C}^1(\mathbb{R}^{2n} \to \mathbb{R}^{2n})$ as in (11) exists and that f_2 in (13) satisfies*

$$f_2(t,y_1,y_2,\eta) = \tilde{f}_2\big(d(t),y_1,y_2,\eta\big) + w(t,y_1,y_2,\eta)$$

for some $d \in \mathscr{L}^\infty(\mathbb{R}_{\geq 0} \to \mathbb{R}^p)$, $\tilde{f}_2 \in \mathscr{C}(\mathbb{R}^p \times \mathbb{R}^{2n} \to \mathbb{R}^{2n-2m})$ and bounded $w \in \mathscr{C}(\mathbb{R} \times \mathbb{R}^{2n} \to \mathbb{R}^{2n-2m})$. Further assume that $\tilde{f}_2$ is locally Lipschitz continuous in η and that the system

$$\dot{\eta}(t) = \tilde{f}_2\big(d(t),y_1(t),y_2(t),\eta(t)\big) + w(t)$$

is input-to-state stable with respect to the input (d,y_1,y_2,w).

We stress that d and w in Assumption 22 typically account for bounded disturbances and noise or modelling errors. In particular, utilizing w in an appropriate way it is possible to incorporate the bounded friction terms (cf. Section 1.2) which may influence the internal dynamics, see also the example discussed in Section 5.1.

Case $r = 3$: The derivation of the internal dynamics is more involved in this case. Following the standard approach presented e.g. in [29, Sec. 5] we may derive a local coordinate transformation to a system of the form

$$y^{(3)}(t) = f_1\big(t,y(t),\dot{y}(t),\ddot{y}(t),\eta(t)\big) \\ \qquad + \Gamma\big(y(t),\dot{y}(t),\ddot{y}(t),\eta(t)\big)u(t), \\ \dot{\eta}(t) = f_2\big(t,y(t),\dot{y}(t),\ddot{y}(t),\eta(t)\big). \tag{14}$$

We omit the details here. Note that in [29] it is assumed that the considered system is time-invariant, i.e., $g(t,q,v) = g(q,v)$, but an extension is possible in our case provided that all conditions hold uniformly with respect to the time t. Now we arrive at the following assumption.

Assumption 23 *We assume that the local diffeomorphism corresponding to the coordinate transformation leading to (14) can be extended to a global diffeomorphism and that f_2 in (14) satisfies*

$$f_2(t,y_1,y_2,y_3,\eta) = \tilde{f}_2\big(d(t),y_1,y_2,y_3,\eta\big) + w(t,y_1,y_2,y_3,\eta)$$

for some $d \in \mathscr{L}^\infty(\mathbb{R}_{\geq 0} \to \mathbb{R}^p)$, $\tilde{f}_2 \in \mathscr{C}(\mathbb{R}^p \times \mathbb{R}^{2n} \to \mathbb{R}^{2n-3m})$ and bounded $w \in \mathscr{C}(\mathbb{R} \times \mathbb{R}^{2n} \to \mathbb{R}^{2n-3m})$. Further assume

that $\tilde{f}_2$ is locally Lipschitz continuous in η and that the system

$$\dot{\eta}(t) = \tilde{f}_2\big(d(t), y_1(t), y_2(t), y_3(t), \eta(t)\big) + w(t)$$

is input-to-state stable with respect to the input (d, y_1, y_2, y_3, w).

3 Servo-constraints approach

The transformed system of (13) or (14) for relative degree $r = 2$ or $r = 3$, respectively, can be used as an inverse model for feedforward control in the control methodology described in Section 1.4. Solving the respective first equation with $y = y_{\text{ref}}$ for the input u yields the feedforward control signal u_{ff} provided the internal dynamics are integrated simultaneously. However, for higher relative degree and multi-input, multi-output systems, the symbolic derivation becomes tedious and complex. Thus, the method of servo-constraints introduced in [11] is applied to demonstrate an alternative. Motivated from modeling of classical mechanical constraints, such as bearing or kinematic loops, the dynamics (1) are appended by m servo-constraints

$$h(q(t)) - y_{\text{ref}}(t) = 0, \tag{15}$$

which enforce the output to stay on the prescribed trajectory $y_{\text{ref}} \in \mathscr{W}^{r,\infty}(\mathbb{R}_{\geq 0} \to \mathbb{R}^m)$. This yields a set of DAEs

$$\begin{aligned}
\dot{q}(t) &= v(t), \\
M\big(q(t)\big)\dot{v}(t) &= g\big(t, q(t), v(t)\big) + B\big(q(t)\big)u(t), \\
0 &= h(q(t)) - y_{\text{ref}}(t) \\
q(0) &= q^0 \in \mathbb{R}^n, \ v(0) = v^0 \in \mathbb{R}^n, \ u(0) = u^0 \in \mathbb{R}^m,
\end{aligned} \tag{16}$$

to be solved numerically for the coordinates q and v and the input u. We stress that the initial values x^0, v^0, u^0 must be chosen so that they are consistent, i.e., a solution of (16) exists. The solution for the input is used as the feedforward control u_{ff}. While classical mechanical constraints are enforced by reaction forces orthogonal to the tangent of the constraint manifold, the servo-constraints are enforced by the generalized input $B\big(q(t)\big)u(t)$ which is not necessarily perpendicular to the tangent of the constraint manifold. Different configurations are distinguished depending on the rank of $\Gamma(q) = H(q)M(q)^{-1}B(q)$, see [12]. In case that $\Gamma(q)$ is of full rank, the system input can directly actuate the output and the inverse model is in so-called orthogonal realization. Note that this means $\Gamma(q) \in \mathbf{Gl}_m(\mathbb{R})$ and hence corresponds to relative degree $r = 2$, cf. Section 1.3. Otherwise, only $\text{rk}\,\Gamma(q)$ components of the system input directly influence the system output and the inverse model is in so-called mixed tangential-orthogonal or purely tangential realization.

While DAEs describing mechanical systems dynamics with classical constraints are of differentiation index 3, the set of DAEs (16) might have a larger differentiation index. As a rule of thumb, the differentiation index is by one larger than the relative degree of the respective system. More precisely, this holds if the internal dynamics is modelled as an ODE and not affected by a constraint, see [16]. This is the case for systems modelled using generalized coordinates as considered here.

The high index DAEs (16) need to be solved numerically, preferably in real-time in order to allow reference trajectories to change in real-time. Since high index DAEs are difficult to solve numerically, see e.g. [23], different index reduction strategies can be applied. In the context of servo-constraints, index reduction by projection is proposed in [12] and minimal extension is proposed in [1,9]. Apart from index reduction techniques, different solvers are applicable to solve the (index reduced) DAE system (16). Possible choices are general high index DAE solvers, e.g. described in [23]. In the context of servo-constraints, the implicit Euler method is proposed in [12]. Alternatively, a reformulation to an optimization scheme is proposed in [2]. The implicit Euler might damp out the internal dynamics and cannot represent them accurately. On the other hand, solving a reformulated optimization problem might not be possible online. Here, we choose a 4-step backwards differencing formula in order to represent the internal dynamics accurately [14]. Real-time applicability and practical realization of the proposed integrator are shown in [33]. In order to verify the numerical solution of (16), it can be compared to the ODE solution of the inverse model represented by either (13) or (14).

The proposed forward time integration of (16) is possible for input-to-state stable internal dynamics which are considered here. Note that the method of servo-constraints is also applicable in the case of unstable internal dynamics when the respective zero dynamics have a hyperbolic equilibrium point at the origin, cf. [17]. Then a stable inversion is possible, which results in solving a boundary value problem or reformulating the boundary value problem to an optimization problem, see [18,39].

4 Funnel control

The feedback control design that we use in the present paper is model-free and hence inherently robust. This is an advantage when we combine it with the feedforward control part. For the feedback part we utilize a combination of a recently developed funnel controller [5] with a funnel precompensator [8]; for details on these individual concepts we refer to the aforementioned works. Here we consider the resulting controller structure as stated in [8] for the two cases of relative degree $r = 2$ and $r = 3$ which reads as follows.

is Hurwitz, i.e., all roots of $p(\lambda)$ have negative real part. Since $p(\lambda)$ is the characteristic polynomial of

$$A = \begin{bmatrix} -q_1 & 1 & & \\ \vdots & & \ddots & \\ -q_{r-1} & & & 1 \\ -q_r & & & 0 \end{bmatrix} \in \mathbb{R}^{r \times r},$$

it follows that A is stable in the sense that all its eigenvalues have negative real part. The constants $p_1, \ldots, p_r > 0$ depend on the choice of the q_i in the following way: Let $Q = Q^\top > 0$ and

$$P = \begin{bmatrix} P_1 & P_2 \\ P_2^\top & P_4 \end{bmatrix}, \quad P_1 \in \mathbb{R}, \ P_2 \in \mathbb{R}^{1 \times (r-1)}, \ P_4 \in \mathbb{R}^{(r-1) \times (r-1)}$$

be such that the Lyapunov equation

$$A^\top P + PA + Q = 0, \quad P = P^\top > 0$$

is fulfilled. The matrix P depends only on the choice of the constants q_i and the matrix Q. The constants p_i must then satisfy

$$\begin{pmatrix} p_1 \\ \vdots \\ p_r \end{pmatrix} = p \cdot P^{-1} \begin{pmatrix} P_1 - P_2 P_4^{-1} P_2^\top \\ 0 \\ \vdots \\ 0 \end{pmatrix} = p \cdot \begin{pmatrix} 1 \\ -P_4^{-1} P_2^\top \end{pmatrix} \quad (20)$$

for some $p > 0$. The purpose of the matrix L_o appearing in (17) and (18) has already been discussed in Section 1.4. The matrix L_i is used to transform the controller output to the physical domain of the input of the to-be-controlled system. Overall, this yields a controller who is internally dealing with dimensionless variables. Further note that the physical dimension of the design parameter $p > 0$ is the reciprocal of time.

The input $u(t)$ of the multibody system (1) is given by the sum of the feedforward control input, the feedback control input and possible input disturbances $u_d \in \mathscr{L}^\infty(\mathbb{R}_{\geq 0} \to \mathbb{R}^m)$, that is

$$\boxed{u(t) = u_{\mathrm{ff}}(t) + u_{\mathrm{fb}}(t) + u_d(t).} \qquad (21)$$

The situation is illustrated in Figure 4. By design, u is also an input of the controllers (17) and (18) which leads to an internal loop in the controller structure. However, this loop may be resolved by inserting (21) as well as the definition of u_{fb} into the differential equations in (17) and (18), respectively. Further inserting the definition of the placeholder variables e_i, which are defined in terms of $z_{i,j}$, $\varphi_i^{(j)}$, $y_{\mathrm{ref}}^{(i)}$ and y, we obtain well defined differential equations. We like to note that the derivatives $\dot{e}_0$ and $\dot{e}_1$ that appear in (17) and (18), which also serve as short-hand notations, may be

---

Case $r = 2$:

$$\dot{z}_1(t) = z_2(t) + \big(q_1 + p_1 k_2(t)\big)\big(L_o y(t) - z_1(t)\big),$$

$$\dot{z}_2(t) = \tilde{\Gamma} L_i^{-1} u(t) + \big(q_2 + p_2 k_2(t)\big)\big(L_o y(t) - z_1(t)\big),$$

$$e_0(t) = z_1(t) - L_o y_{\mathrm{ref}}(t),$$

$$e_1(t) = \dot{e}_0(t) + k_0(t) e_0(t),$$

$$k_0(t) = \frac{1}{1 - \varphi_0(t)^2 \|e_0(t)\|^2},$$

$$k_1(t) = \frac{1}{1 - \varphi_1(t)^2 \|e_1(t)\|^2},$$

$$k_2(t) = \frac{1}{1 - \varphi_2(t)^2 \|L_o y(t) - z_1(t)\|^2},$$

$$u_{\mathrm{fb}}(t) = -k_1(t) L_i e_1(t),$$

(17)

Case $r = 3$:

$$\dot{z}_{1,1}(t) = z_{1,2}(t) + \big(q_1 + p_1 k_3(t)\big)\big(L_o y(t) - z_{1,1}(t)\big),$$

$$\dot{z}_{1,2}(t) = z_{1,3}(t) + \big(q_2 + p_2 k_3(t)\big)\big(L_o y(t) - z_{1,1}(t)\big),$$

$$\dot{z}_{1,3}(t) = \tilde{\Gamma} L_i^{-1} u(t) + \big(q_3 + p_3 k_3(t)\big)\big(L_o y(t) - z_{1,1}(t)\big),$$

$$\dot{z}_{2,1}(t) = z_{2,2}(t) + \big(q_1 + p_1 k_4(t)\big)\big(z_{1,1}(t) - z_{2,1}(t)\big),$$

$$\dot{z}_{2,2}(t) = z_{2,3}(t) + \big(q_2 + p_2 k_4(t)\big)\big(z_{1,1}(t) - z_{2,1}(t)\big),$$

$$\dot{z}_{2,3}(t) = \tilde{\Gamma} L_i^{-1} u(t) + \big(q_3 + p_3 k_4(t)\big)\big(z_{1,1}(t) - z_{2,1}(t)\big),$$

$$e_0(t) = z_{2,1}(t) - L_o y_{\mathrm{ref}}(t),$$

$$e_1(t) = \dot{e}_0(t) + k_0(t) e_0(t),$$

$$e_2(t) = \dot{e}_1(t) + k_1(t) e_1(t),$$

$$k_0(t) = \frac{1}{1 - \varphi_0(t)^2 \|e_0(t)\|^2},$$

$$k_1(t) = \frac{1}{1 - \varphi_1(t)^2 \|e_1(t)\|^2},$$

$$k_2(t) = \frac{1}{1 - \varphi_2(t)^2 \|e_2(t)\|^2},$$

$$k_3(t) = \frac{1}{1 - \varphi_3(t)^2 \|L_o y(t) - z_{1,1}(t)\|^2},$$

$$k_4(t) = \frac{1}{1 - \varphi_4(t)^2 \|z_{1,1}(t) - z_{2,1}(t)\|^2},$$

$$u_{\mathrm{fb}}(t) = -k_2(t) L_i e_2(t),$$

(18)

where

$$y_{\mathrm{ref}} \in \mathscr{W}^{r,\infty}(\mathbb{R}_{\geq 0} \to \mathbb{R}^m), \quad \varphi_i \in \Phi_{r-i}, \ i = 0, \ldots, r-1, \ (19)$$

$\tilde{\Gamma} = \tilde{\Gamma}^\top > 0$, $\varphi_r, \ldots, \varphi_{2r-2} \in \Phi_{r-1}$ and $L_i, L_o \in \mathbf{Gl}_m(\mathbb{R})$. The constants $q_1, \ldots, q_r \in \mathbb{R}$ are such that the polynomial

$$p(\lambda) = \lambda^r + q_1 \lambda^{r-1} + \ldots + q_{r-1} \lambda + q_r$$

resolved using the differential equations in (17) and (18) as follows:

$r = 2$:
$$\dot{e}_0(t) = z_2(t) + \big(q_1 + p_1 k_2(t)\big)\big(L_o y(t) - z_1(t)\big) - L_o \dot{y}_{\text{ref}}(t),$$

$r = 3$:
$$\dot{e}_0(t) = z_{2,2}(t) + \big(q_1 + p_1 k_4(t)\big)\big(z_{1,1}(t) - z_{2,1}(t)\big) - L_o \dot{y}_{\text{ref}}(t),$$
$$\dot{e}_1(t) = z_{2,3}(t) + \big(q_2 + p_2 k_4(t)\big)\big(z_{1,1}(t) - z_{2,1}(t)\big)$$
$$+ p_1 k_4(t)^2 \Big(\varphi_4(t)\dot{\varphi}_4(t)\|z_{1,1}(t) - z_{2,1}(t)\|^2$$
$$+ \varphi_4(t)^2(z_{1,1}(t) - z_{2,1}(t))^\top\big(z_{1,2}(t)$$
$$+ (q_1 + p_1 k_3(t))(L_o y(t) - z_{1,1}(t)) - z_{2,2}(t)$$
$$- (q_1 + p_1 k_4(t))(z_{1,1}(t) - z_{2,1}(t)))\Big)(z_{1,1}(t) - z_{2,1}(t))$$
$$+ \big(q_1 + p_1 k_2(t)\big)\big(z_{1,2}(t) + (q_1 + p_1 k_3(t))(L_o y(t) - z_{1,1}(t))$$
$$- z_{2,2}(t) - (q_1 + p_1 k_4(t))(z_{1,1}(t) - z_{2,1}(t)))$$
$$- L_o \ddot{y}_{\text{ref}}(t) + k_0(t)^2 \Big(\varphi_0(t)\dot{\varphi}_0(t)\|e_0(t)\|^2$$
$$+ \varphi_0(t)^2 e_0(t)^\top \dot{e}_0(t)\Big) e_0(t) + k_0(t)\dot{e}_0(t).$$
$$\tag{22}$$

We stress that the feedback controllers (17) and (18) are model-free, of (comparatively) low complexity, robust with respect to modeling errors, uncertainties and disturbances, and by design they achieve prescribed performance of the tracking error. In a slightly different structure, the controller (17) for the case $r = 2$ was already successfully implemented in [7], see also the discussion therein.

In the following we investigate feasibility of the controllers (17) and (18) in the respective cases. To this end, we define the high-frequency matrix function Γ of the multibody system (1), (2) as follows:

$$r = 2 : \quad \Gamma(q) := H(q)M(q)^{-1}B(q),$$
$$r = 3 : \quad \Gamma(t,q,v) := \Big[H(q)M(q)^{-1}\frac{\partial g}{\partial v}(t,q,v)$$
$$+ \frac{\partial \bar{h}}{\partial v}(q,v)\Big]M(q)^{-1}B(q),$$

for all $t \in \mathbb{R}$ and all $q, v \in \mathbb{R}^n$. For feasibility it is necessary that the high-frequency matrix is constant and, after multiplication with the design parameters L_i and L_o, the product is a positive definite matrix.

Assumption 41 *We assume that the high-frequency matrix satisfies $\Gamma(t,q,v) \equiv \Gamma \in \mathbf{Gl}_m(\mathbb{R})$, and further, $L_o \Gamma L_i = (L_o \Gamma L_i)^\top > 0$.*

We stress that Assumption 41 modifies that made in [5], where Γ is assumed to be positive definite. The reason for this modification is of practical nature: The physical domain of the inputs usually differs from that of the outputs. As a consequence, the quadratic form corresponding to Γ

does not make sense from a physical point of view [31]. The matrices $L_i, L_o \in \mathbf{Gl}_m(\mathbb{R})$ are indeed used to achieve a physical dimension in which only time is involved. Therefore, the quadratic form corresponding to $L_o \Gamma L_i$ is well-defined. Oftentimes, it suffices to choose L_i and L_o as multiples of the identity matrix or as appropriate diagonal matrices. Note that Assumption 41 is satisfied for suitable L_i and L_o, if M, B and $\frac{\partial g}{\partial v}$ are constant and h is linear, but these conditions are not necessary.

Additionally we need to assume that f_1 appearing in (13) and (14) is bounded in t and affine linear in $\dot{y}$ or $(\dot{y}, \ddot{y})$, respectively, and that f_2 in these equations is bounded in $\dot{y}$ or $(\dot{y}, \ddot{y})$, respectively.

Assumption 42 *We assume that f_1 and, in view of Assumptions 22 and 23, $\tilde{f}_2$ in the transformed system (13) and (14), respectively, satisfy*

$$f_1(t, y_1, \ldots, y_r, \eta) = \sum_{i=1}^{r} R_i y_i + \tilde{f}_1\big(d(t), y_1, \eta\big)$$
$$+ v(t, y_1, \ldots, y_r, \eta),$$
$$\tilde{f}_2\big(d(t), y_1, \ldots, y_r, \eta\big) = \bar{f}_2\big(d(t), y_1, \eta\big) + P y_2$$

for $R_i \in \mathbb{R}^{m \times m}$, $i = 1, \ldots, r$, $P \in \mathbb{R}^{(2n-rm) \times m}$, $d \in \mathcal{L}^\infty(\mathbb{R}_{\geq 0} \to \mathbb{R}^p)$, $\tilde{f}_1 \in \mathscr{C}(\mathbb{R}^p \times \mathbb{R}^m \times \mathbb{R}^{2n-rm} \to \mathbb{R}^m)$, $\bar{f}_2 \in \mathscr{C}(\mathbb{R}^p \times \mathbb{R}^m \times \mathbb{R}^{2n-rm} \to \mathbb{R}^{2n-rm})$ and bounded $v \in \mathscr{C}(\mathbb{R} \times \mathbb{R}^{2n} \to \mathbb{R}^m)$ such that the system

$$\dot{\xi}(t) = \bar{f}_2\big(d(t), y_1(t), \xi(t) + P y_1(t)\big) + w(t)$$

is complete with respect to the input (d, y_1, w).

We are now in the position to state the feasibility result.

Theorem 43 *Consider a multibody system (1), (2) with relative degree $r \in \{2, 3\}$ that satisfies Assumption 22 or 23, respectively, the high-frequency matrix satisfies Assumption 41 for some $L_i, L_o \in \mathbf{Gl}_m(\mathbb{R})$, and the involved functions satisfy Assumption 42. Further let $q^0, v^0 \in \mathbb{R}^n$ be initial values, y_{ref} and $\varphi_0, \ldots, \varphi_{r-1}$ be such that (19) holds and $\varphi_r, \ldots, \varphi_{2r-2} \in \Phi_{r-1}$ be such that z_1, e_0, e_1 as defined in (17) or $z_{1,1}, z_{2,1}, e_0, e_1, e_2$ as defined in (18), respectively, satisfy*

$$\varphi_i(0)\|e_i(0)\| < 1, \quad \text{for all } i = 0, \ldots, r-1,$$

and

$$\varphi_2(0)\|L_o y(0) - z_1(0)\| < 1, \quad \text{if } r = 2,$$
$$\varphi_3(0)\|L_o y(0) - z_{1,1}(0)\| < 1$$
$$\text{and} \quad \varphi_4(0)\|z_{1,1}(0) - z_{2,1}(0)\| < 1, \quad \text{if } r = 3.$$

Let $q_1, \ldots, q_r, p_1, \ldots, p_r > 0$ be such that (20) is satisfied for corresponding matrices A, P, Q, and let $\tilde{\Gamma} = \tilde{\Gamma}^\top > 0$ be such that

$$I - L_o \Gamma L_i \tilde{\Gamma}^{-1} = \big(I - L_o \Gamma L_i \tilde{\Gamma}^{-1}\big)^\top > 0 \quad \text{if } r = 3. \tag{23}$$
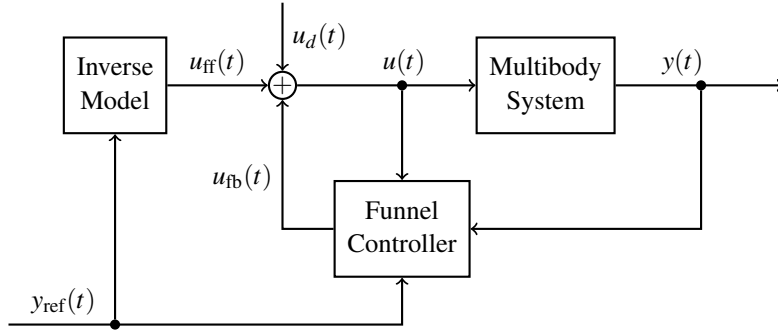
Fig. 4: Controller configuration for the multibody system.

Finally, let $u_{\mathrm{ff}} \in \mathscr{L}^{\infty}(\mathbb{R}_{\geq 0} \to \mathbb{R}^m)$ be the feedforward control input and $u_d \in \mathscr{L}^{\infty}(\mathbb{R}_{\geq 0} \to \mathbb{R}^m)$ be an input disturbance.

Then the application of the funnel controller (17) (if $r = 2$) or (18) (if $r = 3$), respectively, with input defined in (21) to (1), (2) yields an initial-value problem, which has a solution, and every solution can be extended to a maximal solution $(q, v, z) : [0, \omega) \to \mathbb{R}^{2n+mr(r-1)}$, $\omega \in (0, \infty]$, where $z = (z_1, z_2)$ if $r = 2$ and $z = (z_{1,1}, z_{1,2}, z_{1,3}, z_{2,1}, z_{2,2}, z_{2,3})$ if $r = 3$, which has the following properties:

(i) *The solution is global (i.e., $\omega = \infty$).*
(ii) *The input $u : \mathbb{R}_{\geq 0} \to \mathbb{R}^m$, the gain functions $k_0, \ldots, k_{2r-2} : \mathbb{R}_{\geq 0} \to \mathbb{R}$ and q, v, z are bounded.*
(iii) *The functions $e_0, \ldots, e_{r-1} : \mathbb{R}_{\geq 0} \to \mathbb{R}^m$ and the compensator errors $y - z_1$ or $y - z_{1,1}, z_{1,1} - z_{2,1}$, respectively, evolve in their respective performance funnels in the sense*

$$\exists \varepsilon_0, \ldots, \varepsilon_{2r-2} > 0 \, \forall t > 0 :$$
$$\|e_i(t)\| \leq \varphi_i(t)^{-1} - \varepsilon_i, \quad i = 0, \ldots, r-1,$$
$$\|L_o y(t) - z_1(t)\| \leq \varphi_2(t)^{-1} - \varepsilon_2, \quad \text{if } r = 2,$$
$$\|L_o y(t) - z_{1,1}(t)\| \leq \varphi_3(t)^{-1} - \varepsilon_3$$
$$\text{and } \|z_{1,1}(t) - z_{2,1}(t)\| \leq \varphi_4(t)^{-1} - \varepsilon_4, \quad \text{if } r = 3.$$

In particular, the tracking error $e(t) = y(t) - y_{\mathrm{ref}}(t)$ satisfies, for all $t > 0$,

$$\|L_o e(t)\| \leq \varphi_0(t)^{-1} + \varphi_2(t)^{-1} - \varepsilon_0 - \varepsilon_2, \qquad \text{if } r = 2,$$
$$\|L_o e(t)\| \leq \varphi_0(t)^{-1} + \varphi_3(t)^{-1} + \varphi_4(t)^{-1} - \varepsilon_0 - \varepsilon_3 - \varepsilon_4, \quad \text{if } r = 3.$$

Proof Fix $r \in \{2, 3\}$. First note that, due to Assumption 22 or 23, respectively, and Assumptions 41 and 42, system (1), (2) is equivalent to

$$y^{(r)}(t) = \sum_{i=1}^{r} R_i y^{(i-1)}(t) + \tilde{f}_1(d(t), y(t), \eta(t))$$
$$+ v(t, y(t), \ldots, y^{(r-1)}(t), \eta(t)) + \Gamma u(t), \qquad (24)$$
$$\dot{\eta}(t) = P\dot{y}(t) + \bar{f}_2(d(t), y(t), \eta(t))$$
$$+ w(t, y(t), \ldots, y^{(r-1)}(t), \eta(t)).$$

We proceed in several steps.

Step 1: We show that the closed-loop initial value problem has a solution and that it can be extended to a maximal solution. Note that $u_{\mathrm{fb}}(t) = -k_{r-1}(t)L_i e_{r-1}(t)$ from (17) or (18), respectively. Using the same technique as in Step 1 of the proof of [5, Thm. 3.1] it follows that there exist a relatively open set $\mathscr{D} \subseteq \mathbb{R}_{\geq 0} \times \mathbb{R}^{mr}$ and $G \in \mathscr{C}(\mathscr{D} \to \mathbb{R}^m)$ such that

$$u_{\mathrm{fb}}(t) = L_i G(t, e_0(t), \ldots, e_{r-1}(t))$$

and

$$(0, e_0(0), \ldots, e_{r-1}(0)) \in \mathscr{D}.$$

By (22) it then follows that each e_i can be expressed in terms of $L_o y$ and z, hence there exists a function $\tilde{G} \in \mathscr{C}(\tilde{\mathscr{D}} \to \mathbb{R}^m)$, $\tilde{\mathscr{D}} \subseteq \mathbb{R}_{\geq 0} \times \mathbb{R}^{m+mr(r-1)}$ relatively open, such that

$$G(t, e_0(t), \ldots, e_{r-1}(t)) = \tilde{G}(t, L_o y(t), z(t)).$$

Using the notation $Y(t) = (L_o y(t), L_o \dot{y}(t), \ldots, L_o y^{(r-1)}(t))$, the application of the controller (17) or (18), respectively, to (24) with $u(t)$ as in (21) therefore leads to

$$L_o y^{(r)}(t) = \sum_{i=1}^{r} (L_o R_i L_o^{-1}) L_o y^{(i-1)}(t)$$
$$+ L_o \tilde{f}_1(d(t), L_o^{-1}(L_o y(t)), \eta(t))$$
$$+ L_o v(t, \bar{L}_o^{-1} Y(t), \eta(t)) + L_o \Gamma(u_{\mathrm{ff}}(t) + u_d(t))$$
$$+ L_o \Gamma L_i \tilde{G}(t, L_o y(t), z(t)),$$
$$\dot{\eta}(t) = (PL_o^{-1}) L_o \dot{y}(t) + \bar{f}_2(d(t), L_o^{-1}(L_o y(t)), \eta(t))$$
$$+ w(t, \bar{L}_o^{-1} Y(t), \eta(t)),$$
$$\dot{z}(t) = f_3(t, L_o y(t), z(t)),$$
(25)

for some suitable function $f_3 \in \mathscr{C}(\bar{\mathscr{D}} \to \mathbb{R}^{mr(r-1)})$, $\bar{\mathscr{D}} \subseteq \mathbb{R}_{\geq 0} \times \mathbb{R}^{m+mr(r-1)}$ relatively open, and $\bar{L}_o = \mathrm{diag}(L_o, \ldots, L_o)$. It is clear that (25) can be reformulated as a first-order system

$$\frac{\mathrm{d}}{\mathrm{d}t} \begin{pmatrix} Y(t) \\ \eta(t) \\ z(t) \end{pmatrix} = F\left(t, \begin{pmatrix} Y(t) \\ \eta(t) \\ z(t) \end{pmatrix}\right), \quad \begin{pmatrix} Y(0) \\ \eta(0) \\ z(0) \end{pmatrix} = \begin{pmatrix} \bar{L}_o \psi(q^0, v^0) \\ z(0) \end{pmatrix},$$

with a suitable continuous function $F : \hat{\mathscr{D}} \to \mathbb{R}^{2n+mr(r-1)}$, $\hat{\mathscr{D}} \subseteq \mathbb{R}_{\geq 0} \times \mathbb{R}^{2n+mr(r-1)}$ relatively open. Furthermore, $\left(0, \bar{L}_o \psi(q^0, v^0), z(0)\right) \in \hat{\mathscr{D}}$. Hence, by [45, § 10, Thm. IX] there exists a weakly differentiable solution of (25) satisfying the initial conditions and every solution can be extended to a maximal solution; let $(Y, \eta, z) : [0, \omega) \to \mathbb{R}^{2n+mr(r-1)}$, $\omega \in (0, \infty]$, be such a maximal solution.

Step 2: We show that (Y, η, z) also solves a closed-loop system that belongs to the system class defined in [8, (24)]. Set

$$d_1(t) := L_o v\left(t, \bar{L}_o^{-1} Y(t), \eta(t)\right) + L_o \Gamma\left(u_{\mathrm{ff}}(t) + u_d(t)\right),$$

for $t \in [0, \omega)$ and $d_1(t) := 0$ for $t \geq \omega$ (if $\omega < \infty$). Further define

$$d_2(t) := w\left(t, \bar{L}_o^{-1} Y(t), \eta(t)\right), \quad t \in [0, \omega)$$

and $d_2(t) := 0$ for $t \geq \omega$. By the completeness condition from Assumption 42 we may infer that

$$\dot{\xi}(t) = \bar{f}_2\left(d(t), \zeta(t), \xi(t) + PL_o^{-1}\zeta(t)\right) + d_2(t),$$
$$\xi(0) = \Phi(q^0, v^0) - PL_o^{-1} h(q^0),$$

has a solution $\xi(\cdot; \xi(0), d, \zeta, d_2) : [0, \infty) \to \mathbb{R}^{2n-rm}$ for all $\zeta \in \mathscr{C}(\mathbb{R}_{\geq 0} \to \mathbb{R}^m)$. Note that for the maximal solution (Y, η, z) we have that $\xi(\cdot; \xi(0), d, [I_m, 0, \dots, 0]Y, d_2) + PL_o^{-1}[I_m, 0, \dots, 0]Y = \eta$. Now define the operator $T : \mathscr{C}([0, \infty) \to \mathbb{R}^m) \to \mathscr{L}_{\mathrm{loc}}^\infty(\mathbb{R}_{\geq 0} \to \mathbb{R}^{2n-(r-1)m})$ by

$$T(\zeta) := \left(\zeta^\top, \xi(\cdot; \xi(0), d, \zeta, d_2)^\top + (P\zeta)^\top\right)^\top.$$

Clearly, the operator T is causal (property b) in [8, Sec. 3]) and locally Lipschitz continuous (property c) in [8, Sec. 3]). By input-to-state stability, which is due to Assumption 22 or 23, respectively, it follows that boundedness of ζ implies boundedness of $T(\zeta)$. Therefore, we may deduce property a') in [8, Sec. 3]. We may now rewrite (24) using the operator T and equation (21) in the form

$$L_o y^{(r)}(t) = \sum_{i=1}^r (L_o R_i L_o^{-1}) L_o y^{(i-1)}(t) + d_1(t)$$
$$+ L_o \tilde{f}_1\left(d(t), W(TL_o y)(t)\right) - L_o \Gamma L_i k_{r-1}(t) e_{r-1}(t), \tag{26}$$

where $W = \mathrm{diag}\left(L_o^{-1}, I_{2n-rm}\right)$. With $\tilde{d} := (d^\top, d_1^\top)^\top \in \mathscr{L}^\infty(\mathbb{R}_{\geq 0} \to \mathbb{R}^{p+m})$ we find that (26) belongs to the class of systems [8, (24)]. Hence [8, Cor. 4.1] yields feasibility of the controllers (17) and (18), respectively. Since the maximal solution (Y, η, z) is also a maximal solution of (26) it follows that $\omega = \infty$. The statements (ii) and (iii) are also consequences of [8, Cor. 4.1]. □

5 Simulations

We demonstrate the application of the combined feedforward controller, resulting from the servo-constraints approach (16), and feedback controller given by the funnel controller (17) or (18). First, a single-input, single-output system with relative degree $r = 2$ and $r = 3$ is considered. Then, the control methodology is applied to a multi-input, multi-output system with strict relative degree $r = 2$.

5.1 Mass on car system

We consider an example of a mass-spring system mounted on a car from [40], see Figure 5. The mass m_2 moves on a ramp which is inclined by the angle α and mounted on a car with mass m_1, for which it is possible to control the force $u = F$ acting on it. Additional to the considerations in [40] we allow for friction between the mass and the ramp modelled by a friction term as discussed in Section 1.2. The equations of motion for the system are given by

$$\begin{bmatrix} m_1 + m_2 & m_2 \cos\alpha \\ m_2 \cos\alpha & m_2 \end{bmatrix} \begin{pmatrix} \ddot{x}(t) \\ \ddot{s}(t) \end{pmatrix}$$
$$+ \begin{pmatrix} 0 \\ ks(t) + d\dot{s}(t) + F_R(\dot{s}(t)) \end{pmatrix} = \begin{pmatrix} u(t) \\ 0 \end{pmatrix}, \tag{27}$$

where x is the horizontal car position and s the relative position of the mass on the ramp. The constants k, d are the coefficients of the linear spring and damper, respectively. The friction term is given by (5) with parameters $F_0 = 0.31\,\mathrm{N}$, $F_C = 0.16\,\mathrm{N}$, $c_v = 10$, $c_T = 0\,\mathrm{kg/s}$ and $v_{th} = 1 \times 10^{-7}\,\mathrm{m/s}$. The output of the system is given by the horizontal position of the mass on the ramp,
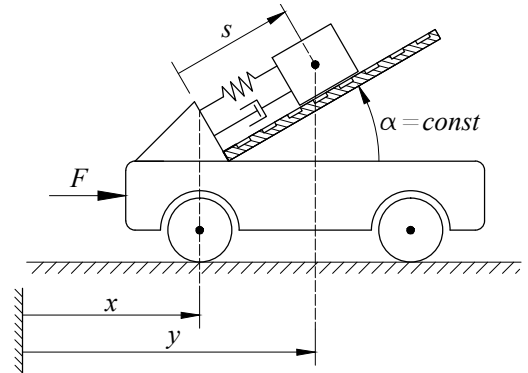
$$y(t) = x(t) + s(t)\cos\alpha. \tag{28}$$

Fig. 5: Mass on car system.

	Inv. model	Sim. model
m_1 (kg)	4	3.6
m_2 (kg)	0.5	0.45
k (N/m)	10	8
d (Ns/m)	0.7	0.6

Table 1: Parameters for the mass on car system.

The parameters chosen for the inverse model and the model for forward simulation are shown in Table 1. The initial values are $x(0) = s(0) = 0$ m and $\dot{x}(0) = \dot{s}(0) = 0$ m/s. We further choose $L_i = 1$ N and $L_o = 1$ m^{-1}.

Clearly, system (27), (28) belongs to the class (1), (2) with a relative degree r depending on the angle α, cf. [40]. Here we consider two cases.

Case 1: If $\alpha = \frac{\pi}{4}$ rad, then system (27), (28) has relative degree $r = 2$ since

$$\Gamma = [1, \cos \alpha] \begin{bmatrix} m_1 + m_2 & m_2 \cos \alpha \\ m_2 \cos \alpha & m_2 \end{bmatrix}^{-1} \begin{bmatrix} 1 \\ 0 \end{bmatrix}$$

$$= \frac{\sin^2 \alpha}{m_1 + m_2 \sin^2 \alpha} \neq 0.$$

We show that Assumptions 22, 41 and 42 are satisfied. Following the procedure to decouple the internal dynamics presented in Section 2, straightforward calculations yield that the diffeomorphism ψ in (11) is given by

$$\psi(q, v) = U \begin{pmatrix} q \\ v \end{pmatrix}, \quad U = \begin{bmatrix} 1 & \cos \alpha & 0 & 0 \\ 0 & 0 & 1 & \cos \alpha \\ \frac{-\cos \alpha}{\sin^2 \alpha} & \frac{-1}{\sin^2 \alpha} & 0 & 0 \\ 0 & 0 & \frac{-\cos \alpha}{\sin^2 \alpha} & \frac{-1}{\sin^2 \alpha} \end{bmatrix},$$

where $(q, v) = (x, s, \dot{x}, \dot{s})$. Hence, the state space transformation $(y, \dot{y}, \eta) = \psi(x, s, \dot{x}, \dot{s})$ of (27), (28) leads to the system (13) given by (29), where $\overline{m} := m_1 + m_2 \sin^2 \alpha$ and $\beta := \frac{\cos \alpha}{\sin^2 \alpha}$. Clearly, Assumption 22 holds with $\tilde{f}_2(d, y_1, y_2, \eta) = Q\eta + R \begin{pmatrix} y_1 \\ y_2 \end{pmatrix}$ and $w(t, y_1, y_2, \eta_1, \eta_2) = \begin{pmatrix} 0 \\ \frac{F_R(-\eta_2 - \beta y_1)}{\sin^2 \alpha} \end{pmatrix}$, since Q only has eigenvalues with negative real part and hence $\dot{\eta}(t) = Q\eta(t) + R \begin{pmatrix} y_1(t) \\ y_2(t) \end{pmatrix} + w(t)$ is input-to-state stable w.r.t. (y_1, y_2, w). Furthermore, Assumption 41 is trivially satisfied and it is easy to see that f_1 and $\tilde{f}_2$ are in the form as required in Assumption 42 and, as a linear system, $\dot{\xi}(t) = Q(\xi(t) + Py(t)) + \bar{P}y(t) + w(t)$ is complete, where $P = R \begin{pmatrix} 0 \\ 1 \end{pmatrix}$ and $\bar{P} = R \begin{pmatrix} 1 \\ 0 \end{pmatrix}$.

The reference trajectory is chosen as the path

$$y_{\text{ref}}(t) = \begin{cases} y_0 + \sigma(t)(y_f - y_0), & t \leq t_f \\ y_f, & t > t_f \end{cases}$$

parameterized by $\sigma(t)$ and with the initial and final values $y_0 = 0$ m and $y_f = 1$ m, respectively. The timing law of the scalar parameter is chosen as

$$\sigma(t) = 70 \left(\frac{t}{t_f}\right)^9 - 315 \left(\frac{t}{t_f}\right)^8 + 540 \left(\frac{t}{t_f}\right)^7$$

$$- 420 \left(\frac{t}{t_f}\right)^6 + 126 \left(\frac{t}{t_f}\right)^5 \tag{30}$$

with final transition time $t_f = 1.8$ s. For the controller (17) we choose the initial values $z_1(0) = 0$, $z_2(0) = 0$ s^{-1}, which coincide with the initial value of the reference trajectory and the funnel functions

$$\varphi_0(t) = \varphi_2(t) = 2(e^{-5\text{s}^{-1}t} + 0.02)^{-1},$$

$$\varphi_1(t) = (e^{-10\text{s}^{-1}t} + 0.1)^{-1},$$

and $\tilde{\Gamma} = 0.15$ s^{-2}. The parameters q_i, p_i are determined by the coefficients of the Hurwitz polynomial

$$(\lambda + 5\text{s}^{-1})^2 = \lambda^2 + 10\text{s}^{-1}\lambda + 25\text{s}^{-2},$$

by which $q_1 = 10$ s^{-1} and $q_2 = 25$ s^{-2}. Therefore, $A = \begin{bmatrix} -10\text{s}^{-1} & 1 \\ -25\text{s}^{-2} & 0 \end{bmatrix}$ and the Lyapunov equation $A^\top P + PA = -\text{diag}(1\text{s}^{-1}, 1\text{s})$ has the solution

$$P = \begin{bmatrix} \frac{13}{10} & -\frac{1}{2}\text{s} \\ -\frac{1}{2}\text{s} & \frac{63}{250}\text{s}^2 \end{bmatrix},$$

by which the choice $p = 1$ s^{-1} leads to $p_1 = 1$ s^{-1} and $p_2 = \frac{125}{63}$ s^{-2}. Obviously the initial errors lie within the respective funnel boundaries and therefore all assumptions of Theorem 43 are satisfied, thus it yields that the combination of feedforward control by servo-constraints and funnel controller (17) is feasible.

We compare three different simulation scenarios. To this end, we assume that the actual system (27) is subject to modelling errors in its parameters and that the friction force F_R is unknown (and hence assumed to be zero in the reference model for feedforward control). The perturbed parameters for the actual model used in forward simulation are also shown in Table 1. In the first scenario C1, the combination of the feedforward control input computed from the servo-constraints approach and the feedback control input determined by the funnel controller (17) is applied to the system. In the second scenario C2, only the funnel controller (17) is applied to the system. And in the third scenario C3, only the feedforward control input is applied to the actual system.

The simulations over the time interval $0 - 3$ s were performed in MATLAB (solver: ode15s, rel. tol.: 10^{-14}, abs. tol.: 10^{-10}) and are depicted in Figure 6. The performance funnel and the tracking errors for scenarios C1–C3 are shown in Figure 6a, while the output is shown in Figure 6b and the input signals generated by the controllers in each

$$\ddot{y}(t) = \frac{m_1 \cos \alpha}{m_2 \overline{m}} \left[k\eta_1(t) + d\eta_2(t) + k\beta y(t) + d\beta \dot{y}(t) - F_R\left(-\eta_2(t) - \beta \dot{y}(t) \right) \right] + \frac{\sin^2 \alpha}{\overline{m}} u(t),$$

$$\begin{pmatrix} \dot{\eta}_1(t) \\ \dot{\eta}_2(t) \end{pmatrix} = \underbrace{\begin{bmatrix} 0 & 1 \\ \frac{-k}{m_2 \sin^2 \alpha} & \frac{-d}{m_2 \sin^2 \alpha} \end{bmatrix}}_{=:Q} \begin{pmatrix} \eta_1(t) \\ \eta_2(t) \end{pmatrix} + \underbrace{\begin{bmatrix} 0 & 0 \\ \frac{-k\beta}{m_2 \sin^2 \alpha} & \frac{-d\beta}{m_2 \sin^2 \alpha} \end{bmatrix}}_{=:R} \begin{pmatrix} y(t) \\ \dot{y}(t) \end{pmatrix} + \begin{pmatrix} 0 \\ \frac{F_R\left(-\eta_2(t) - \beta \dot{y}(t) \right)}{\sin^2 \alpha} \end{pmatrix}, \tag{29}$$

scenario are depicted in Figure 6c. It can be seen that the feedforward control input in scenario C3 is not able to achieve tracking performance within the prescribed funnel boundaries in the presence of the modelling errors and unknown friction. It should be noted that in case of no errors and disturbances, the feedforward control achieves perfect tracking. On the other hand, if only the funnel controller is applied as in scenario C2, then the tracking error stays within the performance funnel, however the generated input signal has some undesired peaks. When the feedforward control is combined with the funnel controller as in scenario C1, then it can be seen that the desired tracking performance is achieved and the input signal does not vary as strongly as in scenario C2; in particular, no high peaks are present.

For the favorable scenario C1, the states x and s are depicted in Figure 7a, and the spring force F_S, the damping force F_D and the friction F_R are shown in Figure 7b. It can be seen that sudden changes in the friction force F_R are present which can cause peaks in the feedback control input.

Case 2: If $\alpha = 0\,$rad, then system (27), (28) has relative degree $r = 3$ since

$$\Gamma(\dot{s}) = [1, \cos \alpha] \begin{bmatrix} m_1 + m_2 & m_2 \cos \alpha \\ m_2 \cos \alpha & m_2 \end{bmatrix}^{-1} \begin{bmatrix} 0 & 0 \\ -k & -d - F_R'(\dot{s}) \end{bmatrix}$$

$$\times \begin{bmatrix} m_1 + m_2 & m_2 \cos \alpha \\ m_2 \cos \alpha & m_2 \end{bmatrix}^{-1} \begin{bmatrix} 1 \\ 0 \end{bmatrix}$$

$$= \frac{d + F_R'(\dot{s})}{m_1 m_2} \neq 0.$$

However, $F_R'(\dot{s})$ is not well-defined at each $\dot{s}$, and in order to satisfy Assumption 41 we require that Γ is constant. Therefore, we assume in this case that the friction is not present, i.e., $F_R = 0\,$N in the inverse model as well as the actual model in forward time simulation. The other parameters are equal to the ones used in Case 1, see Table 1. It is then a simple exercise (similar to Case 1) to show that Assumptions 23, 41 and 42 are satisfied, which is hence left to the reader.

The reference trajectory is chosen as

$$y_{\mathrm{ref}}(t) = \begin{cases} \frac{61}{3} \left(\frac{t}{t_s} \right)^9 - \frac{563}{6} \left(\frac{t}{t_s} \right)^8 + 166 \left(\frac{t}{t_s} \right)^7 - \\ \frac{403}{3} \left(\frac{t}{t_s} \right)^6 + \frac{127}{3} \left(\frac{t}{t_s} \right)^5 \,\mathrm{m}, & t \leq t_s \\ 0.5 \cos(t - t_s)\,\mathrm{m}, & t > t_s, \end{cases}$$

which ensures a smooth transition from the initial position $y_{\mathrm{ref}}(0) = 0\,$m to a cosine oscillation at $t_s = 2\,$s with an amplitude of $0.5\,$m. For the controller (18) we choose the initial values $z_{i,j}(0) = 0\,\mathrm{s}^{-j+1}$, $i = 1, 2$, $j = 1, 2, 3$, the funnel functions

$$\varphi_0(t) = \varphi_3(t) = \varphi_4(t) = 3(e^{-2\mathrm{s}^{-1}t} + 0.02)^{-1},$$
$$\varphi_1(t) = (2e^{-10\mathrm{s}^{-1}t} + 0.05)^{-1},$$
$$\varphi_2(t) = (2e^{-20\mathrm{s}^{-1}t} + 0.005)^{-1}$$

and $\tilde{\Gamma} = 0.4\mathrm{s}^{-3}$. We note that (23) is satisfied since, using the actual system parameters, $\Gamma = \frac{d}{m_1 m_2} \approx 0.37/\mathrm{kgs}$, and thus $L_o \Gamma L_i \approx 0.37\mathrm{s}^{-3} < \tilde{\Gamma}$. The parameters q_i, p_i are determined by the coefficients of the Hurwitz polynomial

$$(\lambda + 5\mathrm{s}^{-1})^3 = \lambda^3 + 15\mathrm{s}^{-1}\lambda^2 + 75\mathrm{s}^{-2}\lambda + 125\mathrm{s}^{-3},$$

by which $q_1 = 15\mathrm{s}^{-1}$, $q_2 = 75\mathrm{s}^{-2}$ and $q_3 = 125\mathrm{s}^{-3}$. Therefore, $A = \begin{bmatrix} -15\mathrm{s}^{-1} & 1 & 0 \\ -75\mathrm{s}^{-2} & 0 & 1 \\ -125\mathrm{s}^{-3} & 0 & 0 \end{bmatrix}$ and the Lyapunov equation $A^\top P + PA = -\mathrm{diag}\left(1\mathrm{s}^{-1}, 1\mathrm{s}, 1\mathrm{s}^3\right)$ has the solution

$$P = \begin{bmatrix} \frac{58}{5} & -\frac{1}{2}\mathrm{s} & -\frac{136}{125}\mathrm{s}^2 \\ -\frac{1}{2}\mathrm{s} & \frac{136}{125}\mathrm{s}^2 & -\frac{1}{2}\mathrm{s}^3 \\ -\frac{136}{125}\mathrm{s}^2 & -\frac{1}{2}\mathrm{s}^3 & \frac{1333}{3125}\mathrm{s}^4 \end{bmatrix},$$

by which the choice $p = 1\mathrm{s}^{-1}$ leads to $p_1 = 1\mathrm{s}^{-1}$, $p_2 = \frac{1383}{391}\mathrm{s}^{-2}$ and $p_3 = \frac{2230}{333}\mathrm{s}^{-3}$. The initial errors lie within the respective funnel boundaries. All assumptions of Theorem 43 are satisfied, thus it yields that the combination of feedforward control by servo-constraints and funnel controller (18) is feasible.

We compare the same three simulation scenarios as in Case 1, with the same parameter variations of the simulation model. Note that the funnel controller (18) is used instead of (17) due to a relative degree $r = 3$ in this case. Moreover, we stress that the reference trajectory is different in this case as it is not a smooth working point change but rather a smooth transition to a cosine oscillation.

The simulations over the time interval $0 - 10\mathrm{s}$ were performed in MATLAB (solver: ode15s, rel. tol.: 10^{-14}, abs. tol.: 10^{-10}) and are depicted in Figure 8 for scenarios C1–C3. The tracking errors are shown in Figure 8a, the system output in Figure 8b and the input signals in Figure 8c. Similar to Case 1, it can be seen that the tracking error in
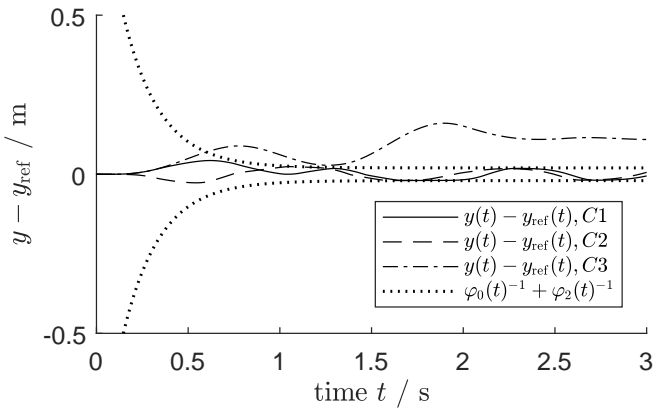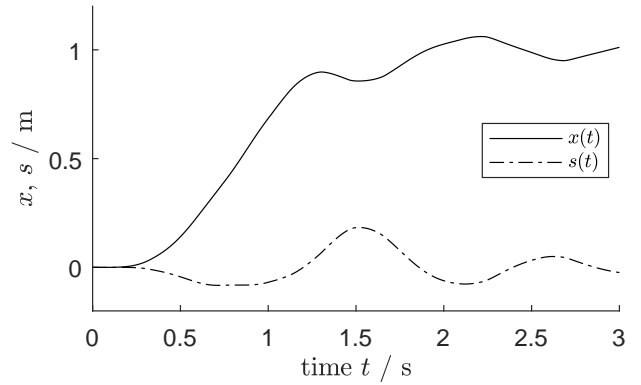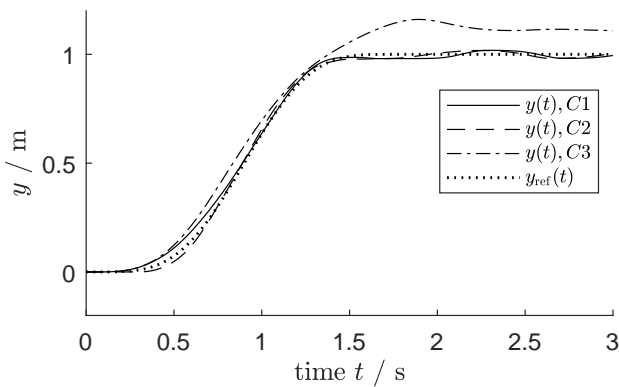
Fig. 6a: Funnel and tracking errors

Fig. 6b: System output
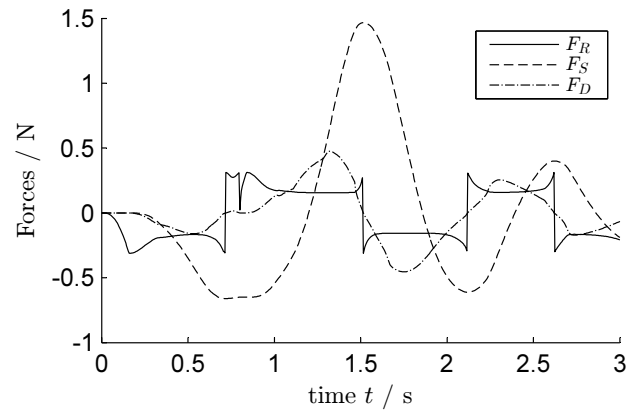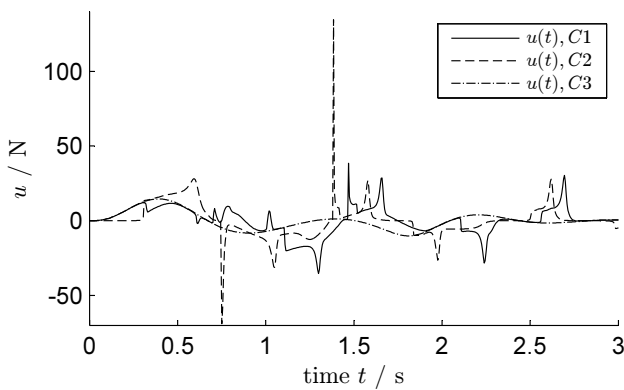

Fig. 6c: Control inputs

Fig. 6: Simulation of feedforward and feedback controllers for the system (27) with $\alpha = \frac{\pi}{4}$ rad.

scenario C3 (only feedforward) leaves the prescribed performance funnel, and the input signal in scenario C2 (only feedback) has undesired peaks when compared to the input signals generated in the other scenarios. In the end, the com-

Fig. 7a: States

Fig. 7b: Forces

Fig. 7: States and forces for the combination of feedforward and feedback controllers for the system (27) with $\alpha = \frac{\pi}{4}$ rad.

bination of feedforward control and funnel controller as in scenario C1 seems again the favorable choice.

For scenario C1, the states x and s are depicted in Figure 9a, and the spring force F_S and damping force F_D are shown in Figure 9b. It can be seen that strong variations of the forces at the beginning cause strong variations of the feedback control input.

5.2 Planar robotic manipulator

We consider an example of a robotic manipulator as depicted in Figure 10. The robotic manipulator is planar and consists of three rigid bodies. Bodies 2 and 3 model a rotational manipulator arm connected by a passive joint. The passive joint is modelled as a rotational spring-damper combination with spring coefficient k and damping coefficient d. The arm is connected to body 1 that moves on a linear axis. Two actuators are available for control. The first actuator u_1
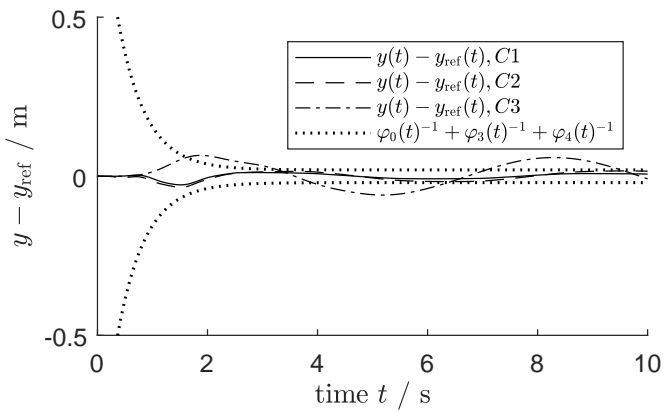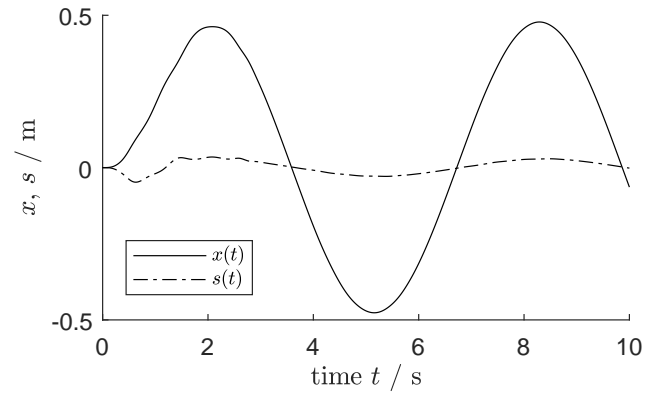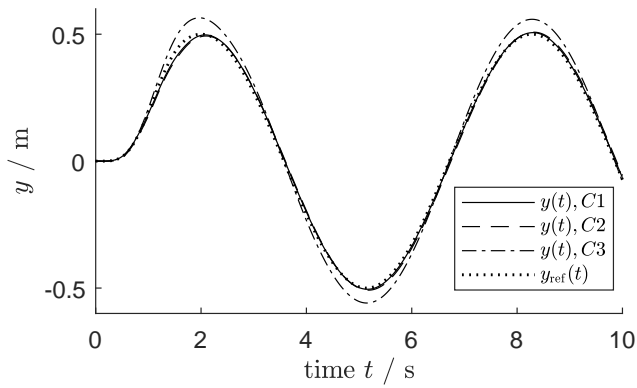
Fig. 8a: Funnel and tracking errors

Fig. 8b: System output

Fig. 8c: Control inputs

Fig. 8: Simulation of feedforward and feedback controllers for the system (27) with $\alpha = 0\,\mathrm{rad}$.

Fig. 9a: States
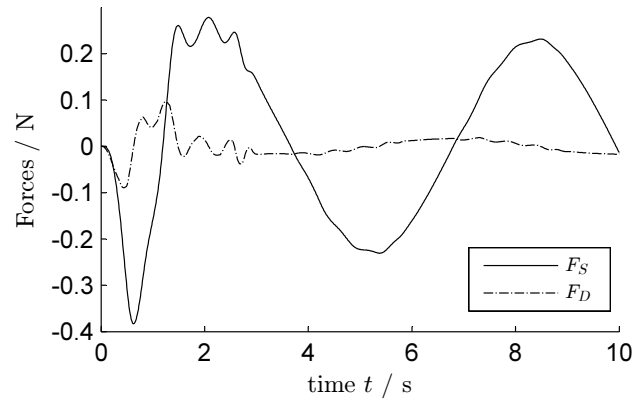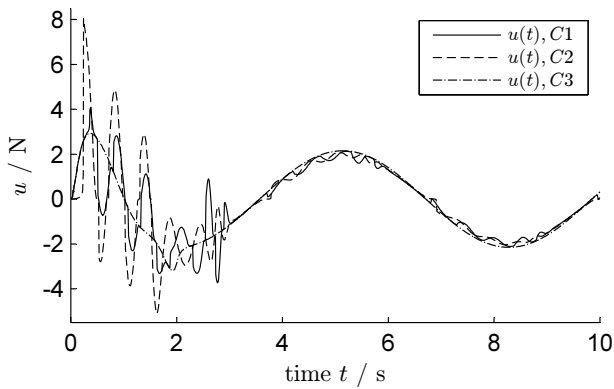

Fig. 9b: Forces

Fig. 9: States and forces for the combination of feedforward and feedback controllers for the system (27) with $\alpha = 0\,\mathrm{rad}$.

the mass m_1 and the linear axis by a friction term as discussed in Section 1.2.
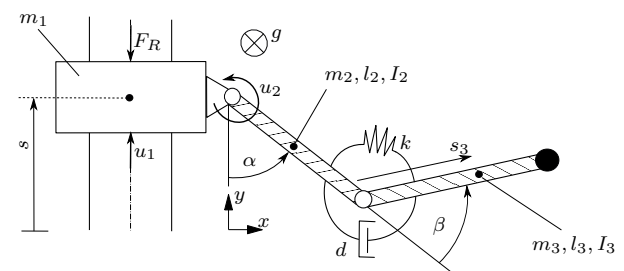
Fig. 10: Planar rigid revolute joint robotic manipulator.

moves body 1 on the linear axis, while the second actuator u_2 rotates the first manipulator arm. Thus, the system is underactuated. Additionally, we allow for friction between

The first body is of mass m_1, the second and third body are of mass m_2 and m_3 with length l_2 and l_3 and moment of inertia $\mathscr{I}_2$ and $\mathscr{I}_3$, respectively. The center of gravity of body 3 is denoted by s_3, as depicted in Fig-

ure 10. The friction term $F_R(\dot{s})$ is given by (5) with parameters $F_0 = 0.49\,\text{N}$, $F_C = 0.25\,\text{N}$, $c_v = 10$, $c_T = 0\,\text{kg/s}$ and $v_{th} = 1 \times 10^{-7}\,\text{m/s}$. The vector of generalized coordinates is chosen as

$$q(t) = \begin{bmatrix} s(t) \\ \alpha(t) \\ \beta(t) \end{bmatrix}, \tag{31}$$

where s denotes the position of body 1, and the angular rotation of bodies 2 and 3 is described by α and β, respectively. The output of the multibody system is the end effector position calculated by

$$r(t) = \begin{bmatrix} l_2 \sin(\alpha(t)) + l_3 \sin(\alpha(t) + \beta(t)) \\ s(t) - l_2 \cos(\alpha(t)) - l_3 \cos(\alpha(t) + \beta(t)) \end{bmatrix}. \tag{32}$$

The equations of motion are derived using the Newton-Euler formalism [37] and are of the form (1) with g, M, B given in (33). As proposed in [38], the output (32) is linearized for small angles β in order to simplify the analysis of the internal dynamics. For small angle β, an auxiliary angle γ of the end effector position

$$\gamma(t) = \alpha(t) + \frac{l_3}{l_2 + l_3}\beta(t)$$

is introduced. This yields the approximated end effector position

$$r_{\text{app}}(t) = \begin{bmatrix} (l_2 + l_3)\sin(\gamma(t)) \\ s(t) - (l_2 + l_3)\cos(\gamma(t)) \end{bmatrix}.$$

The end effector position can be obtained from the new output $y(t)$ which is linear in the states and can be split into actuated and unactuated coordinates

$$y(t) = \begin{bmatrix} s(t) \\ \alpha(t) \end{bmatrix} + \begin{bmatrix} 0 \\ \frac{l_3}{l_2 + l_3}\beta(t) \end{bmatrix}. \tag{34}$$

The system (1) with output (34) has relative degree 2 since

$$\Gamma(\alpha, \beta) = \begin{bmatrix} 1 & 0 & 0 \\ 0 & 1 & \frac{l_3}{l_2 + l_3} \end{bmatrix} M(\alpha, \beta)^{-1} \begin{bmatrix} 1 & 0 \\ 0 & 1 \\ 0 & 0 \end{bmatrix} \in \mathbf{Gl}_2(\mathbb{R}).$$

However, for the standard location of the center of gravity of body 3, $s_3 = \frac{l_3}{2}$, the internal dynamics are unstable. Note that in [38], a slightly different manipulator with fixed base and 4 links is considered. Nevertheless, the internal dynamics of the passive last link are similar to the system considered here. It is proposed in [38] to optimize the parameters of the last link, namely mass m_3, position s_3 and its moment of inertia $\mathscr{I}_3$, to obtain input-to-state stable internal dynamics. From a mechanical design point of view, this can for example be realized by adding counterweights. The optimization result is taken from [38]. The parameters used for the simulation are summarized in Table 2 for the inverse model for

	Inv. model	Sim. model
d (Nms/rad)	0.5	0.4
k (Nm/rad)	120	100
m_1(kg)	3	3
m_2 (kg)	3.438	3.438
$\mathscr{I}_2$ (kgm^2)	0.0723	0.0723
l_2 (m)	0.5	0.5
m_3 (kg)	3.969	4.3659
$\mathscr{I}_3$ (kgm^2)	0.2434	0.2434
s_3 (m)	0.172	0.172

Table 2: Simulation parameters for robotic manipulator.

feedforward control as well as the simulation model used for forward time simulation.

While the crucial structural assumptions for the application of our controller design are satisfied, Theorem 43 is not applicable here since Assumption 41 is not satisfied as the matrix $\Gamma(\alpha, \beta)$ is not constant. Nevertheless, the simulations show that the our approach is feasible and the combination of feedforward controller and funnel controller works. This may serve as a motivation for future research to extend Theorem 43 to larger classes of systems which do not necessarily satisfy the Assumptions 22, 41 and 42.

For the simulation we have chosen $L_i = \text{diag}(1\text{mkg}\,\text{s}^{-2}, 1\text{m}^2\,\text{kg}\,\text{s}^{-2})$, $L_o = \text{diag}(1\text{m}^{-1}, 1\text{rad}^{-1})$ (and hence $L_i\Gamma(\alpha, \beta)L_o$ is always positive definite) and the straight reference path

$$r_{\text{ref},i}(t) = \begin{cases} r_{0,i} + \sigma(t)(r_{f,i} - r_{0,i}), & t \leq t_f \\ r_{f,i}, & t > t_f \end{cases} \tag{35}$$

for each component $i \in \{1, 2\}$ of the end effector position $r(t)$, where the initial and final end effector positions are denoted by r_0 and r_f, respectively. The path is parameterized by the scalar parameter $\sigma(t) \in [0, 1]$, which has a timing law given by the same polynomial as in (30) with transition time $t_f = 6.4\,\text{s}$. This ensures a smooth transition between the initial end effector position r_0 and the final end effector position r_f which are chosen as

$$r_0 = \begin{bmatrix} l_2 + l_3 \\ 0 \end{bmatrix} \quad \text{and} \quad r_f = \begin{bmatrix} \sin(\alpha_f)(l_2 + l_3) \\ -\cos(\alpha_f)(l_2 + l_3) \end{bmatrix}$$

with a final angle $\alpha_f = \frac{\pi}{6}\text{rad}$. The initial values of the robotic manipulator are chosen as $s(0) = 0\,\text{m}, \alpha(0) = \frac{\pi}{2}\text{rad}, \beta(0) = 0\,\text{rad}, \dot{s}(0) = 0\,\text{m/s}, \dot{\alpha}(0) = \dot{\beta}(0) = 0\,\text{rad/s}$, which coincide with the desired trajectory.

For the controller (17) we choose the initial values $z_1(0) = (0, \frac{\pi}{2})$, $z_2(0) = (0, 0)\text{s}^{-1}$, the funnel functions

$$\varphi_0(t) = \varphi_2(t) = 2(5e^{-2\text{s}^{-1}t} + 0.05)^{-1},$$
$$\varphi_1(t) = (5e^{-10\text{s}^{-1}t} + 0.05)^{-1},$$

$$
M(\alpha,\beta) = \begin{bmatrix}
m_1+m_2+m_3 & m_3(s_3\sin(\alpha+\beta)+l_2\sin(\alpha))+\frac{l_2m_2\sin(\alpha)}{2} & m_3s_3\sin(\alpha+\beta) \\
m_3(s_3\sin(\alpha+\beta)+l_2\sin(\alpha))+\frac{l_2m_2\sin(\alpha)}{2} & \mathscr{I}_2+\mathscr{I}_3+\frac{l_2^2m_2}{4}+l_2^2m_3+m_3s_3^2+2l_2m_3s_3\cos(\beta) & m_3s_3^2+l_2m_3\cos(\beta)s_3+\mathscr{I}_3 \\
m_3s_3\sin(\alpha+\beta) & m_3s_3^2+l_2m_3\cos(\beta)s_3+\mathscr{I}_3 & m_3s_3^2+\mathscr{I}_3
\end{bmatrix},
$$

$$
g(\dot{s},\alpha,\beta,\dot{\alpha},\dot{\beta}) = \begin{bmatrix}
-m_3(\dot{\beta}(\dot{\alpha}s_3\cos(\alpha+\beta)+\dot{\beta}s_3\cos(\alpha+\beta))+\dot{\alpha}(\dot{\alpha}(s_3\cos(\alpha+\beta)+l_2\cos(\alpha))+\dot{\beta}s_3\cos(\alpha+\beta)))-\frac{l_2\dot{\alpha}^2m_2\cos(\alpha)}{2}-F_R(\dot{s}) \\
l_2\dot{\beta}m_3s_3\sin(\beta)(2\dot{\alpha}+\dot{\beta}) \\
-l_2m_3s_3\sin(\beta)\dot{\alpha}^2-d\dot{\beta}-k\beta
\end{bmatrix},
$$

$$
B = \begin{bmatrix} 1 & 0 \\ 0 & 1 \\ 0 & 0 \end{bmatrix}
$$

(33)

and $\tilde{\Gamma} = \operatorname{diag}(0.1,0.7)\mathrm{s}^{-3}$. The parameters q_i, p_i are chosen as in Case 1 in Section 5.1 as $q_1 = 10\mathrm{s}^{-1}$, $q_2 = 25\mathrm{s}^{-2}$ and $p_1 = 1\mathrm{s}^{-1}$, $p_2 = \frac{125}{63}\mathrm{s}^{-2}$. Obviously the initial errors lie within the respective funnel boundaries.

We compare the same three simulation scenarios as described in Case 1 in Section 5.1; in particular, the friction is assumed to be unknown and therefore zero in the inverse model for feedforward control. Moreover, we assume that system (1) is subject to modelling errors in the spring and damper constants and the mass m_3, see Table 2. The perturbed mass is chosen to be 10% larger than the mass of the inverse model.

The simulations over the time interval $0 - 8\mathrm{s}$ were performed in MATLAB (solver: ode15s, rel. tol.: 10^{-14}, abs. tol.: 10^{-10}) and are depicted in Figure 11 and Figure 12 for the corresponding scenarios C1–C3. The funnel boundary and the tracking errors are shown in Figure 11a, while the end effector position $r(t)$ as in (32) and reference $r_{\mathrm{ref}}(t)$ in the x,y coordinate system are shown in Figure 11b. The components of the input signals are shown in Figure 12a and b. It can be seen that the tracking error in scenario C3 (only feedforward) deviates very much from the desired tracking performance determined by the performance funnel. This is mainly due to the friction arising in the simulation model which is not present in the inverse model. The input signal in scenario C2 (only feedback) varies strongly and has undesired peaks, especially when compared to the input signal generated by the combination of feedforward control and funnel controller as in scenario C1. Therefore, the latter seems the favorable choice.

For scenario C1, the states s, α, β are depicted in Figure 13a, and the spring force F_S, the damping force F_D and the friction force F_R are shown in Figure 13b. It can be seen that the friction force F_R is dominates the spring and damper forces. However, the controller is still able to keep the tracking error in the performance funnel.
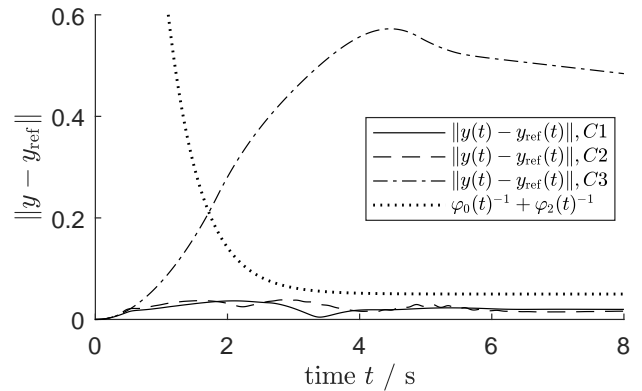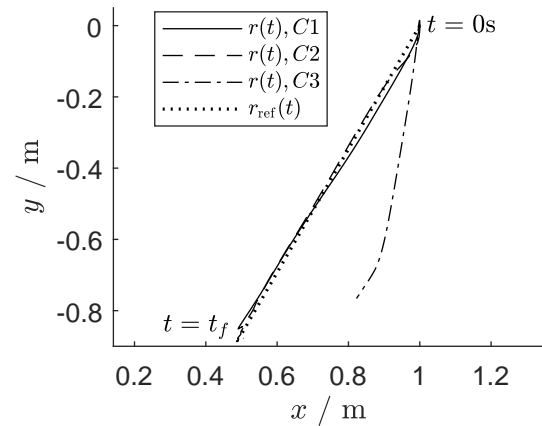

Fig. 11a: Funnel and tracking errors

Fig. 11b: End effector position and reference

Fig. 11: Simulation of feedforward and feedback controllers for the system (1) with output (34).

6 Conclusions

We have considered the problem of tracking with prescribed transient behavior of the tracking error for multibody systems which are modelled using generalized coordinates.
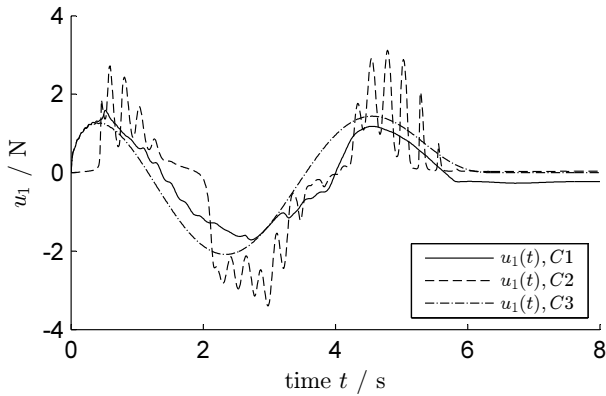
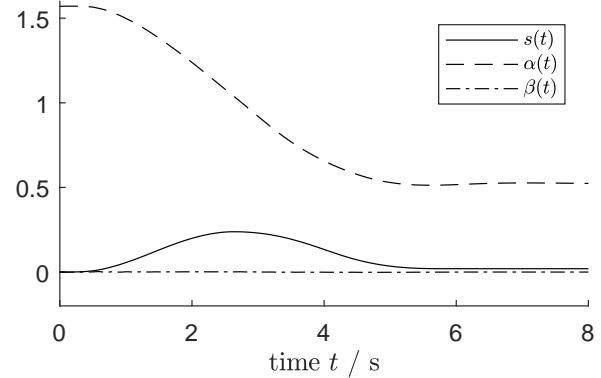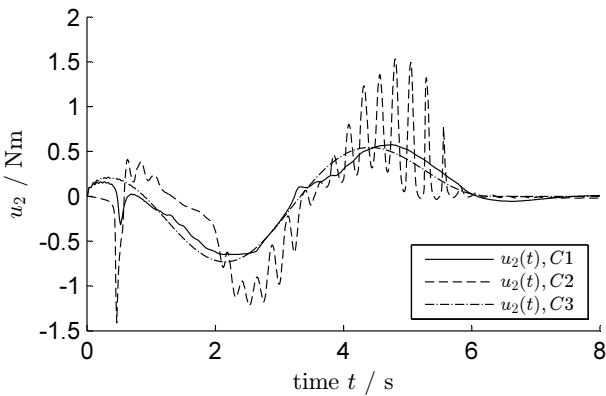Fig. 12a: First components of control input

Fig. 12b: Second components of control input

Fig. 12: Simulation of feedforward and feedback controllers for the system (1) with output (34).
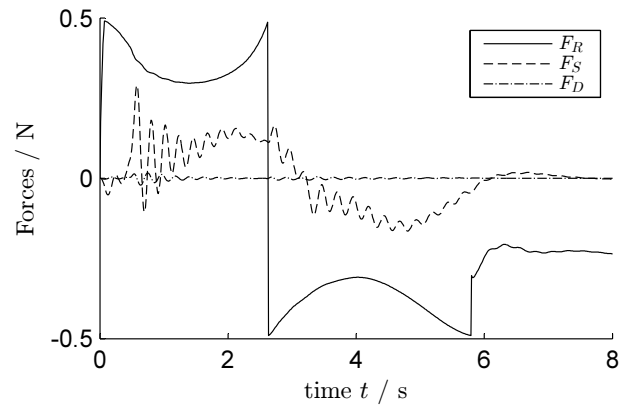

Fig. 13a: States

Fig. 13b: Forces

Fig. 13: States and forces for the combination of feedforward and feedback controllers for the system (1) with output (34).

Friction terms were explicitly allowed in the model. We restricted ourselves to systems with relative degree two or three which have input-to-state stable internal dynamics. The latter assumption was made precise in Section 2, where the internal dynamics of the multibody systems had been decoupled. Following the two degree of freedom controller design approach we combined a feedforward with a feedback controller. Using the method of servo-constraints, the feedforward control input was computed on the basis of an inverse model, see Section 3. The feedback controller is the combination of a recently developed funnel controller [5] with a funnel pre-compensator [8]. The latter is a favorable choice, since the resulting dynamic output feedback is model-free and hence inherently robust. In Section 4 we have proved the feasibility of the controller design. The results were illustrated by some typical examples of a mass on car system and a planar robotic manipulator in Section 5.

Future research should focus on relaxing the Assumptions 41 and 42 which restrict the application of the con-

troller design. This became apparent in Case 2 in Section 5.1, where we needed to assume that the friction is absent in order to satisfy the assumptions. Furthermore, the example of the robotic manipulator in Section 5.2 did not satisfy the assumptions, but nevertheless we obtained satisfying results using the proposed control design.

References

1. Altmann, R., Betsch, P., Yang, Y.: Index reduction by minimal extension for the inverse dynamics simulation of cranes. Multibody Sys. Dyn. **36**(3), 295–321 (2016)
2. Altmann, R., Heiland, J.: Simulation of multibody systems with servo constraints through optimal control. Multibody Sys. Dyn. **40**(1), 75–98 (2017)
3. Armstrong-Hélouvry, B., Dupont, P.E., Canudas-de Wit, C.: A survey of models, analysis tools and compensation methods for the control of machines with friction. Automatica **30**(7), 1083–1138 (1994)

4. Berger, T.: On differential-algebraic control systems. Ph.D. thesis, Institut für Mathematik, Technische Universität Ilmenau, Universitätsverlag Ilmenau, Germany (2014).

5. Berger, T., Lê, H.H., Reis, T.: Funnel control for nonlinear systems with known strict relative degree. Automatica **87**, 345–357 (2018). DOI 10.1016/j.automatica.2017.10.017

6. Berger, T., Reis, T.: Zero dynamics and funnel control for linear electrical circuits. J. Franklin Inst. **351**(11), 5099–5132 (2014)

7. Berger, T., Reis, T.: Funnel control via funnel pre-compensator for minimum phase systems with relative degree two. IEEE Trans. Autom. Control **63**(7), 2264–2271 (2018). DOI 10.1109/TAC.2017.2761020

8. Berger, T., Reis, T.: The Funnel Pre-Compensator. Int. J. Robust & Nonlinear Control (2018). To appear

9. Betsch, P., Altmann, R., Yang, Y.: Numerical integration of underactuated mechanical systems subjected to mixed holonomic and servo constraints. In: J.M. Font-Llagunes (ed.) Multibody Dynamics, *Computational Methods in Applied Sciences*, vol. 42, pp. 1–18. Springer-Verlag, Cham (2016). DOI 10.1007/978-3-319-30614-8_1

10. Betsch, P., Quasem, M., Uhlar, S.: Numerical integration of discrete mechanical systems with mixed holonomic and control constraints. J. Mech. Sci. Tech. **23**(4), 1012–1018 (2009)

11. Blajer, W.: Index of differential-algebraic equations governing the dynamics of constrained mechanical systems. Appl. Math. Mod. **16**(2), 70–77 (1992)

12. Blajer, W., Kołodziejczyk, K.: A geometric approach to solving problems of control constraints: Theory and a DAE framework. Multibody Sys. Dyn. **11**(4), 343–364 (2004)

13. Blajer, W., Kołodziejczyk, K.: Improved DAE formulation for inverse dynamics simulation of cranes. Multibody Sys. Dyn. **25**(2), 131–143 (2011)

14. Brenan, K.E., Campbell, S.L., Petzold, L.R.: Numerical Solution of Initial-Value Problems in Differential-Algebraic Equations. North-Holland, Amsterdam (1989)

15. Byrnes, C.I., Isidori, A.: A frequency domain philosophy for nonlinear systems, with application to stabilization and to adaptive control. In: Proc. 23rd IEEE Conf. Decis. Control, vol. 1, pp. 1569–1573 (1984)

16. Campbell, S.L.: High-index differential algebraic equations. Mechanics of Structures and Machines **23**(2), 199–222 (1995)

17. Chen, D., Paden, B.: Stable inversion of nonlinear non-minimum phase systems. Int. J. Control **64**(1), 81–97 (1996)

18. Devasia, S., Chen, D., Paden, B.: Nonlinear inversion-based output tracking. IEEE Trans. Autom. Control **41**(7), 930–942 (1996)

19. Fumagalli, A., Masarati, P., Morandini, M., Mantegazza, P.: Control constraint realization for multibody systems. J. Comput. Nonlinear Dynam. **6**(1), 011,002–011,002–8 (2010)

20. Gear, C.W.: Differential-algebraic equation index transformations. SIAM J. Sci. Stat. Comput. **9**, 39–47 (1988)

21. Gross, D., Hauger, W., Schröder, J., Wall, W.: Technische Mechanik 1: Statik, 13 edn. Springer-Verlag, Berlin-Heidelberg (2016)

22. Hackl, C.M.: Non-identifier Based Adaptive Control in Mechatronics–Theory and Application, *Lecture Notes in Control and Information Sciences*, vol. 466. Springer-Verlag, Cham, Switzerland (2017)

23. Hairer, E., Wanner, G.: Solving ordinary differential equations II: Stiff and differential-algebraic problems, *Springer Series in Computational Mathematics*, vol. 14, 2nd edn. Springer-Verlag, Berlin (1996)

24. Ilchmann, A.: Decentralized tracking of interconnected systems. In: K. Hüper, J. Trumpf (eds.) Mathematical System Theory - Festschrift in Honor of Uwe Helmke on the Occasion of his Sixtieth Birthday, pp. 229–245. CreateSpace (2013)

25. Ilchmann, A., Mueller, M.: Time-varying linear systems: Relative degree and normal form. IEEE Trans. Autom. Control **52**(5), 840–851 (2007)

26. Ilchmann, A., Ryan, E.P.: High-gain control without identification: a survey. GAMM Mitt. **31**(1), 115–125 (2008)

27. Ilchmann, A., Ryan, E.P., Sangwin, C.J.: Tracking with prescribed transient behaviour. ESAIM: Control, Optimisation and Calculus of Variations **7**, 471–493 (2002)

28. Ilchmann, A., Trenn, S.: Input constrained funnel control with applications to chemical reactor models. Syst. Control Lett. **53**(5), 361–375 (2004)

29. Isidori, A.: Nonlinear Control Systems, 3rd edn. Communications and Control Engineering Series. Springer-Verlag, Berlin (1995)

30. Kunkel, P., Mehrmann, V.: Differential-Algebraic Equations. Analysis and Numerical Solution. EMS Publishing House, Zürich, Switzerland (2006). DOI 10.4171/017

31. Langhaar, H.: Dimensional Analysis and Theory of Models. John Wiley and Sons Inc., New York (1951)

32. Leine, R.I., Nijmeijer, H.: Dynamics and bifurcations of non-smooth mechanical systems, *Lecture notes in applied and computational mechanics*, vol. 18. Springer-Verlag, Berlin-Heidelberg (2004)

33. Otto, S., Seifried, R.: Analysis of servo-constraints solution approaches for underactuated multibody systems. In: Proc. IMSD Lisbon 2018, Submitted to proceedings IMSD 2018 (2017)

34. Otto, S., Seifried, R.: Open-loop control of underactuated mechanical systems using servo-constraints: Analysis and some examples. Tech. rep., Institute of Mechanical and Ocean Engineering, Hamburg University of Technology (2017). Submitted to DAE Forum

35. Otto, S., Seifried, R.: Real-time trajectory control of an overhead crane using servo-constraints. Multibody Sys. Dyn. **42**(1), 1–17 (2018). DOI 10.1007/s11044-017-9569-4

36. Pomprapa, A., Weyer, S., Leonhardt, S., Walter, M., Misgeld, B.: Periodic funnel-based control for peak inspiratory pressure. In: Proc. 54th IEEE Conf. Decis. Control, Osaka, Japan, pp. 5617–5622 (2015)

37. Schiehlen, W., Eberhard, P.: Applied dynamics. Springer-Verlag, Switzerland (2014)

38. Seifried, R.: Integrated mechanical and control design of underactuated multibody systems. Nonlinear Dynamics **67**(2), 1539–1557 (2012)

39. Seifried, R.: Two approaches for feedforward control and optimal design of underactuated multibody systems. Multibody Syst. Dyn. **27**, 75–93 (2012)

40. Seifried, R., Blajer, W.: Analysis of servo-constraint problems for underactuated multibody systems. Mech. Sci. **4**, 113–129 (2013)

41. Senfelds, A., Paugurs, A.: Electrical drive DC link power flow control with adaptive approach. In: Proc. 55th Int. Sci. Conf. Power Electr. Engg. Riga Techn. Univ., Riga, Latvia, pp. 30–33 (2014)

42. Skogestad, S., Postlethwaite, I.: Multivariable Feedback Control: Analysis and Design, 2nd edn. John Wiley and Sons Inc., Chichester (2005)

43. Sontag, E.D.: Smooth stabilization implies coprime factorization. IEEE Trans. Autom. Control **34**(4), 435–443 (1989)

44. Sontag, E.D.: On the input-to-state stability property. European J. Control **1**, 24–36 (1995)

45. Walter, W.: Ordinary Differential Equations. Springer-Verlag, New York (1998)